# Human neurogenesis is altered via glucocorticoid-mediated regulation of *ZBTB16* expression

Anthi C. Krontira[1,2,*], Cristiana Cruceanu[1,3], Leander Dony[1,2,7,8], Christina Kyrousi[4,5,6], Marie-Helen Link[1], Nils Kappelmann[1,2], Dorothee Pöhlchen[1,2], Catarina Raimundo[1], Signe-Penner Goeke[1], Alicia Schowe[1,9], Darina Czamara[1], Marius-Lahti-Pulkkinen[10,11,12], Sara Sammallahti[13], Elina Wolford[10], Kati Heinonen[10,14,15], Simone Roeh[1], Vincenza Sportelli[1], Barbara Wölfel[1], Maik Ködel[1], Susann Sauer[1], Monika-Rex-Haffner[1], Katri Räikkönen[10], Marta Labeur[1], Silvia Cappello[4], Elisabeth B. Binder[1]

1. Department of Translational Research in Psychiatry, Max Planck Institute of Psychiatry, Munich, Germany, 80804 Munich, Germany
2. International Max Planck Research School for Translational Psychiatry, Munich, Germany, 80804 Munich, Germany
3. Department of Physiology and Pharmacology, Karolinska Institutet, Stockholm Sweden
4. Developmental Neurobiology, Max Planck Institute of Psychiatry, 80804 Munich, Germany
5. First Department of Psychiatry, Medical School, National and Kapodistrian University of Athens, Eginition Hospital, Greece
6. University Mental Health, Neurosciences and Precision Medicine Research Institute "Costas Stefanis", Athens, Greece
7. Department for Computational Health, Helmholtz Munich, 85764 Neuherberg, Germany
8. TUM School of Life Sciences Weihenstephan, Technical University of Munich, 85354 Freising, Germany
9. Graduate School of Systemic Neurosciences, Ludwig-Maximilians-University, 82152 Munich, Germany
10. Department of Psychology and Logopedics, Faculty of Medicine, University of Helsinki, 00014 Helsinki, Finland
11. Finnish Institute for Health and Welfare, 00271 Helsinki, Finland
12. Centre for Cardiovascular Science, Queen's Medical Research Institute, University of Edinburgh, Edinburgh EH16 4TJ, UK
13. Department of Obstetrics and Gynecology, Helsinki University Hospital and University of Helsinki, 00014 Helsinki, Finland
14. Psychology/Welfare, Faculty of Social Sciences, University of Tampere, Tampere, Finland
15. Lawrence S. Bloomberg Faculty of Nursing, University of Toronto, Toronto, Canada

* Current address: Götz lab, Institute for Stem Cell Research, Helmholtz Zentrum Munich, Germany

**Co-corresponding authors**

Elisabeth B. Binder: binder@psych.mpg.de & Anthi C. Krontira: anthi_krontira@psych.mpg.de

**Summary**

Glucocorticoids are important for proper organ maturation and their levels are tightly regulated during development. Here we use human cerebral organoids and mice to study cell-type specific effects of glucocorticoids on neurogenesis. We show that glucocorticoids increase a specific type of basal progenitors (co-expressing *PAX6* and *EOMES*) that has been shown to drive cortical expansion in gyrified species. This effect is mediated via the transcription factor *ZBTB16* and leads to increased production of neurons. A phenome-wide mendelian randomization analysis of an enhancer variant that moderates glucocorticoid-induced *ZBTB16* levels, reveals causal relationships with higher educational attainment and altered brain structure. The relationship with postnatal cognition is supported by data from a prospective pregnancy cohort. This study provides a novel cellular and

molecular pathway for the effects of glucocorticoids on human neurogenesis that relates to lasting postnatal phenotypes.

**Keywords**

Glucocorticoids, *ZBTB16*, cerebral organoids, developing mouse, dexamethasone, progenitors, gyrified species, neurogenesis, ITU cohort, mendelian randomization

## Introduction

Prenatal development relates to postnatal health. The 'developmental origin of health and disease (DOHaD) hypothesis'[1] proposes that environmental exposures during critical prenatal periods have lasting effects on cells and tissues impacting human health throughout life. This is also true for the central nervous system (CNS) with a number of environmental factors shown to impact its cellular architecture and function[2].

An important factor for CNS development during pregnancy are glucocorticoids (GCs)[3]. These steroid hormones, the main one being cortisol in humans, are endogenously present prenatally. They regulate fetal organ development and maturation, being especially important for lung and brain[4]. GC levels are very tightly regulated during gestation in a species-specific pattern. While there is a physiological rise of GCs close to term in most species that is important for final organ development and parturition, their levels throughout gestation differ. For example, corticosterone, the main GC in mice, exhibits a sharp increase late in gestation, between embryonic day 16 and 17, while in humans cortisol levels increase progressively during gestation starting at the beginning of the second trimester[5].

GCs are found increased outside the physiological range and/or time-window due to the therapeutic use of synthetic GCs (sGCs) during pregnancy but also as a result of endocrine and stress-related disorders of the mother[3]. The placenta constitutes a protective barrier for endogenous maternal GCs, with only as little as 10% of the maternal circulating hormones reaching the fetal compartments. This barrier has been shown to be affected by maternal stress and depression resulting in reduced placental cortisol metabolism[6]. Furthermore, sGCs readily cross the placenta[7] leading to higher exposure of the fetus. sGCs, either betamethasone or dexamethasone, are most commonly prescribed starting at 22 and until 33 gestational weeks (GWs) in pregnancies with high risk for preterm delivery to facilitate fetal lung maturation[8]. More than 1 in 10 babies are born prematurely every year, a number which amounts to ~15 million preterm births (< GW37) per year[9] of which ~ 615,000 are born extremely preterm (< GW28)[10], highlighting the clinical and societal importance of prenatal sGCs use. sGC treatment has also been associated with a 3.5-fold increase of survival rates in preterm infants born at GW22[11], highlighting the importance of an even more extensive use of sGCs in extremely preterm births. Given the clear anti-inflammatory effects of sGCs, they were also used during the COVID-19 pandemic in patients requiring oxygen therapy and mechanical ventilation[12]. Pregnant women were not excluded from this treatment course, with the guidelines specifically promoting the use of dexamethasone in women that fulfill the afore-mentioned criteria[13].

Exposure to levels of prenatal GCs outside of the physiological range has been related to lasting postnatal effects at the behavioral and brain structural levels[14]. While the effects of steroids on brain structure and function may also be mediated by inflammatory agents, direct effects are supported by data from animal models. In fact, the overall molecular and cellular effects of GCs on the term and adult brain are well-characterized in rodents[15]. Interestingly, their impact on early stages of brain development and especially during the neurogenic period, which extends until GW28[16] in humans and thus in the timeframe of sGC administration for extremely preterm births, have rarely been studied and are absent for the human brain or complex models of the human developing cortex. To address this important question, we combined experiments in human cerebral organoids (hCOs) and mouse embryos with human genetic analyses and mechanistically linked enhanced prenatal sGC exposure to human cortical neurogenesis and possibly to lasting effects on mental and cognitive abilities and brain structure.

88

89 **Results**

90 **Glucocorticoids increase the number of basal progenitors**

91 To study GC regulation of neurogenic trajectories in the developing neocortex we treated hCOs[17] for 7 days with
92 100nM of dexamethasone (dex), a dose and time consistent with therapeutic guidelines followed in clinical settings[8]
93 (see Methods for detailed explanation). This treatment was initiated at day 43 (Figure 1A) in hCOS derived from 2
94 independent iPSC (induced pluripotent stem cell) lines. Days 40-50 were chosen as a time-range when hCOs are
95 actively performing neurogenic processes with all the progenitor cell types present while birth of deep layer neurons
96 is peaking and of upper layer neurons has started[18]. First, we analyzed the specific effects of dex on different
97 progenitor cell types defined by the expression of PAX6 (Paired Box 6) and EOMES (Eomesodermin - also known
98 as T-box brain protein 2 or TBR2). PAX6 is highly expressed in radial glia (RG) cells, EOMES, but not PAX6, in
99 intermediate basal progenitors (IPs), while both can be expressed in certain basal progenitors (BPs). Dex
100 consistently led to a significant increase of PAX6+EOMES+ BPs (Figure 1B,C) in hCOs derived from both iPSC
101 lines compared to veh-treated hCOs. The increased PAX6+EOMES+ BPs were localized at the basal side of the
102 germinal zones, in the subventricular-like zone (SVZ) (Figure 1D and Figure S1A,B). Moreover, we confirmed the
103 effects of dex on the increase of double-positive BPs by analyzing the number of PAX6+EOMES-, PAX6-EOMES+
104 and PAX6+EOMES+ progenitor subtypes in No.1- hCOs with flow cytometry analysis (FCa). We observed a
105 significant increase (+11%) in PAX6+EOMES+ BPs when hCOs were treated with dex compared to veh (Figure
106 S2A-C). Co-administration of the glucocorticoid receptor (GR) antagonist RU486 supported that dex effects are
107 mainly mediated by the GR and not the mineralocorticoid receptor (Figure S2A,D,E). To study whether dex
108 treatment affected the transcriptomic profile of PAX6+EOMES+ BPs we generated and analyzed single-cell RNA
109 sequencing (sc-RNA seq) data of HPS0076 hCOs treated with 100nM of dex for 10 days (treatment initiation at day
110 60). We found a 3.38-fold increase in the numbers of the PAX6+EOMES+ cells after dex, similar to the fold changes
111 we found with our immunostaining analysis (Figure S1C). Interestingly, gene set enrichment analysis of the
112 differentially expressed (DE) genes between treatment groups in these double positive cells pinpointed gene sets
113 associated with cell fate commitment and glia cell proliferation and differentiation (Figure S1D & Tables S2,3),
114 highlighting the importance of these cells in regulating neurogenic processes (see Supplemental Results for more
115 details).

116 We next sought to characterize the effects of dex on different neuronal populations. To this end, we labeled deep-
117 layer VI and V neurons with TBR1 (T-box brain transcription factor) and BCL11B (BAF Chromatin Remodeling
118 Complex Subunit- also known as CTIP2) respectively and upper layer IV neurons with SATB2 (SATB Homeobox
119 2, Figure 1E). Dex consistently led to a significant increase of upper-layer SATB2 positive neurons in hCOs derived
120 from both iPSC lines compared to veh-treated ones. No significant change was found in deep layer neurons (Figure
121 1F). To further validate these results we used FCa and found increased numbers of upper-layer IV neurons
122 (SATB2+ cells, 9% significant increase, Figure S3A,B) following dex. In addition, dex led to an increase of immature
123 neuronal somata (doublecortin, DCX+) at the basal parts of the germinal zone (Figure S3C,D) and to a decrease
124 of the DCX zone thickness in the cortical-like plate (CP, Figure S3C,E), potentially pointing to later-born neurons
125 still migrating to their final destination. This putatively prolongated neurogenesis can be related to the increased
126 numbers of PAX6+EOMES+ BPs. These BPs have high proliferative capacity, undergoing not only neurogenic but
127 also self-renewing proliferative divisions, which comes in contrast to PAX6-EOMES+ IPs that primarily undergo one
128 neurogenic division producing two neurons[19–24]. Interestingly, PAX6+EOMES+ BPs are abundant in the inner and
129 outer SVZ of mammals with a gyrified brain, such as ferrets, primates and humans, and are one of the mechanisms
130 responsible for the increased neurogenic potential of these species[20]. In lissencephalic species, like rodents, this
131 cell type is rare with the vast majority of BPs being IPs[19–24]. Overall, GCs seem to increase neurogenic processes

132 that are enriched in gyrified species, highlighting the importance of steroid hormones in regulating developmental
133 processes.
134
135 **Transcriptional response to glucocorticoids during neurogenesis**
136 We next aimed to identify genes and pathways responsible for the effects of GCs on neurogenesis. For this we
137 used bulk RNA sequencing of No.1- day 45 hCOs following the exact treatment paradigm as above (100nM of dex
138 or vehicle for 7 days, treatment start at day 38). At a 10% FDR cutoff, fifty genes were DE (Table S4). Given the
139 essential role and developmental specificity of transcription factors (TFs) in determining neurodevelopmental
140 processes[25], we decided to focus on this class of proteins. Out of the 50 DE genes only 4 were TFs, *TSC22D3*
141 (TSC22 Domain family member 3), *KLF9* (Kruppel-like factor 9), *ZBTB16* (Zinc finger and BTB domain-containing
142 protein 16) and *HEYL* (HEY-like protein) (Figure 1G). To narrow in on progenitor-specific responses, we used two
143 scRNA seq datasets. First, to define cell-type specific expression of these TFs we used an already published
144 dataset of No1 day 30 hCOs[26]. *HEYL* and *KLF9* were very lowly expressed in the majority of cell types, *TSC22D3*
145 was found across all cell types and only the expression *ZBTB16* coincided with *PAX6* positive cells (Figure S4D,E
146 and Table S8). To study cell-type specific effects of extended dex treatment on these TFs we used the scRNA seq
147 dataset of HPS0076 hCOs with chronic dex stimulation. *ZBTB16* was differentially overexpressed only in the Radial
148 glia and Cycling progenitors clusters (Figure 1I,J & Table S5), and thus the strongest candidate for dex effects on
149 neural progenitors. *ZBTB16* (also known as *PLZF*- promyelocytic leukemia zinc finger protein) has been associated
150 with regulation of the balance between self-renewal and differentiation of stem and progenitor cells in multiple organ
151 systems including the brain[27]. Thus, we decided to focus on this TF. It belongs to the Krüppel-like zinc finger family
152 of TFs and is very well conserved across species. It has nine zinc finger motifs in the C terminus that comprise the
153 DNA binding domain of the protein, a protein-protein interaction domain at the N terminus and a less well
154 characterized middle RD2 (repressor domain 2) domain and can act as a transcriptional activator or repressor[27].
155
156 **Glucocorticoids alter the very dynamic neurodevelopmental expression pattern of *ZBTB16***
157 *ZBTB16* is dynamically expressed during rodent and human neurodevelopment with high brain expression early in
158 gestation and a subsequent downregulation to low levels. In rodents, *Zbtb16* is expressed until E10.5 (embryonic
159 day 10.5) in the forebrain[28] when it is downregulated to non-detectable levels during neurogenesis (Figure S4A,B).
160 In contrast, in human fetal cortex *ZBTB16* is expressed during the initial stages of neurogenesis (Figure S4C),
161 indicating expression of this TF during the neurogenic period in humans but not in rodents.
162 We analyzed the ZBTB16 expression pattern in our model of the developing human neocortex, the hCOs. ZBTB16
163 was dynamically expressed in hCOs with high RNA (Figure 2A) and protein (Figure 2B) levels at the early stages
164 of organoid development, until approximately day 40, with a subsequent decrease when mature neurons emerge
165 (MAP2+ cells, Microtubule-associated protein 2) (day 50, Figure 2A). We found ZBTB16 enriched in the apical and
166 basal side of the VZ, mainly expressed by progenitor cells (SOX2+ cells, SRY-Box Transcription Factor 2) and not
167 expressed by mature neurons (MAP2+) (Figure 2C). Thus, *ZBTB16* exhibits a very dynamic expression pattern in
168 hCOs with high protein expression during the initial period of neurogenesis, consistent with data reported from
169 human fetal cortex (Figure S4C).
170 Given the specificity of *ZBTB16* expression in progenitor clusters, we took advantage of the chronic scRNA seq
171 data to investigate the effects of *ZBTB16* expression in the transcriptional signature of progenitor cells. We sub-
172 setted our dataset to the progenitor clusters in the vehicle condition and performed a DE analysis for ZBTB16-
173 positive versus negative cells (Table S6). We found 442 DE genes at a nominal p-value cutoff of 0.05, one of which
174 was PAX6 (p-value 0.003). Gene Set Enrichment analysis revealed significantly enriched gene sets associated with

175 neuron differentiation, regulation of microtubule organization and transcription highlighting the importance of
176 *ZBTB16* in regulating proliferative and neurogenic processes (Figure S4F, Table S7).
177 Next, we examined the levels of ZBTB16 expression after dex administration in hCOs (100nM dex, for 7 days
178 starting at day 43- Figure S5A). Treatment with dex resulted in increased expression of *ZBTB16* at the RNA level
179 (Figure S5B, similar to what we have previously reported after 4- and 12- hours dex treatments[26]) and at the protein
180 level (Figure 2D,E) in the progenitor cells that line the ventricular-like zone (VZ, Figure S5C,D). This strongly
181 resembles what we observed at a single-cell genome wide level (Figure 1I,J). In fact, dex alters the tightly-regulated
182 developmental expression pattern of this TF by reversing its levels to those of day 30 and younger hCOs (Figure
183 2F). Together, these results suggest that dex maintains high *ZBTB16* expression during later stages of
184 neurogenesis, at developmental time-windows with physiologically lower levels of this TF, in the progenitor cells
185 that line the germinal zones.
186
187 ***ZBTB16* mimics the effects of glucocorticoids on basal progenitors**
188 To test whether the effect of dex on BPs is mediated via *ZBTB16*, we overexpressed ZBTB16 and GFP from a
189 bicistronic plasmid or GFP from a monocistronic control plasmid, in hCOs starting at day 43 when ZBTB16
190 expression is already declining (Figure 2A,B). Subsequent analyses were performed 7 days after the
191 electroporation, at day 50 (Figure 3A). In order to explore effects on progenitor subtypes of the VZ and the SVZ and
192 on neurons of the CP, we divided the electroporated area in three bins of equal height starting from the most apical
193 part of the VZ and stopping at the outermost electroporated cell in the CP and analysed the effects of ZBTB16
194 overexpression on GFP+ electroporated cells.
195 ZBTB16 overexpression led to increased numbers of Ki67+ cells (Figure 3B,C), indicating an increase in
196 proliferation potential. In analogy to the experiments with dex, we next co-analyzed PAX6 and EOMES expression.
197 Indeed, ZBTB16 overexpression led to a similar phenotype to that of dex, with an overall 25.7% increase in
198 PAX6+EOMES+ BPs (Figure 3D,E) in bins B and C (Figure 3F, 23.8% increase in bin B and 43.1% increase in bin
199 C), which reflect the basal parts of the VZ, the SVZ and the CP. Interestingly, there was a substantial increase of
200 these BPs in bin C (43.1%) which associates to the CP of the organoids, pointing to a potential identity change of
201 this bin to resemble an area with cells typically found in the inner and outer SVZ of gyrencephalic species. Using
202 GFP cell morphology reconstructions, we found that the double-positive BPs exhibit both IP-related morphologies
203 with no processes and bRG-related morphologies with monopolar or bipolar cells (Figure S6, see Supplemental
204 Results for more details), similar to what has been described before for these double positive cells in macaques
205 and humans[20,29].
206 We next studied the effects of ZBTB16 overexpression on deep-layer V and upper-layer IV neurons by staining with
207 BCL11B and SATB2 respectively. We found a significant 19% increase of SATB2+ cells after ZBTB16
208 overexpression (Figure S7B,C), whereas the effect of dex on BCL11B+ deep-layer neurons was less-pronounced
209 (non-significant 11% increase, Figure S7A,C), indicating increased neuronal production. Thus, ZBTB16
210 overexpression increases the amount of double-positive BPs and of upper-layer neurons, effects that resemble the
211 ones of dex (Figure 1E,F).
212
213 ***ZBTB16* is necessary for the effects of glucocorticoids on basal progenitors**
214 In view of the similarity of the dex and ZBTB16 overexpression phenotypes on BPs, we sought to determine whether
215 ZBTB16 is in fact necessary for the dex-induced phenotype. To achieve this, we used CRISPR-Cas9 to knock-out
216 (KO) exon 2 of the *ZBTB16* locus in the No.1- iPSCs. Exon 2 encodes for more than 50% of the protein and includes
217 the initiating ATG, the BTB/POZ domain and the first two zinc fingers of the binding domain[30]. We created
218 heterozygous No.1- (from now on called ZBTB16$^{+/-}$) iPSCs where one allele of the *ZBTB16* locus is wild-type and

219 one allele has exon 2 excised. A full KO of exon 2 in both alleles was not viable at the iPSC cell stage. We then
220 treated ZBTB16$^{+/+}$- derived (CRISPR control No.1- iPSCs) and ZBTB16$^{+/-}$-derived day 43 hCOs with 100nM dex for
221 7 days and analysed ZBTB16 protein expression as well as the relative abundance of PAX6+EOMES-, PAX6-
222 EOMES+ and PAX6+EOMES+ progenitor subtypes with FCa and immunofluorescence at day 50 (Figure 4A).
223 ZBTB16$^{+/-}$ hCOS showed significantly less increase of the ZBTB16 protein following dex treatment than the
224 ZBTB16$^{+/+}$ hCOs (46% less increase, Figure 4B,C). FCa of the ZBTB16$^{+/+}$ hCOs validated the increase of
225 PAX6+EOMES+ BPs under dex treatment (Figure 4D,E- 22.2% increase, similarly to what we found with the No.1
226 wild-type hCOs (Figure S2B,C). However, in the ZBTB16$^{+/-}$ hCOs, the number of double-positive BPs was not
227 significantly increased in the dex condition in respect to veh (Figure 4F,G- 6% non-significant increase). This was
228 further validated at the immunofluorescence level where dex significantly increased the numbers of
229 PAX6+EOMES+ BPs in ZBTB16$^{+/+}$ hCOs but not in ZBTB16$^{+/-}$ hCOs (Figure S8), recapitulating the effects we see
230 with our FC analysis. Together, these results indicate that ZBTB16 is necessary for the effects of GCs on
231 PAX6+EOMES+ BPs and suggests that it could potentially play a key role in the maintenance of the
232 PAX6+EOMES+ BP population in gyrified species under baseline conditions.
233
234 **Heterochronic *ZBTB16* expression in mouse fetal brain is sufficient to induce basal progenitors typically**
235 **enriched in gyrified species and increase neurogenesis**
236 While the principles of neurogenesis are similar among all mammalian species, differences exist in respect to their
237 temporal progression as well as to the different progenitor subtypes populating the SVZ which play a key role in the
238 overall neurogenic potential. In lissencephalic species BPs double-positive for PAX6 and EOMES are very rare[19],
239 the neurogenic period is much shorter[31] (9 days in mice compared to 110 days in humans) and *ZBTB16* is not
240 physiologically expressed at any point during the neurogenic period (Figure S4C,D). In order to analyse if altered
241 expression of *ZBTB16* during neurogenesis would lead to increased numbers of PAX6+EOMES+ BPs also in a
242 lissencephalic species, we performed *in utero* electroporations at E13.5 in mouse brains with the same plasmids
243 as for the hCOs and analysed the effects of human *ZBTB16* overexpression at E16.5 (Figure 5A). Considering the
244 more complex cortical cellular architecture of the mouse brain as compared to hCOs, we divided the electroporated
245 area in five bins of equal height where bin A includes the VZ and the SVZ, bin B the SVZ and intermediate zone
246 (IZ), bin C the IZ and bins D and E the CP.
247 In mice, ZBTB16 overexpression significantly changed the distribution of the GFP+ electroporated cells.
248 ZBTB16+GFP+ cells accumulated in the SVZ with less cells reaching the outer-most part of the cortical plate (Figure
249 5B,C), indicating possible identity changes and/or altered timing of differentiation. Similar to hCOs, we found more
250 Pax6+Eomes+ BPs (Figure 5D,E, 8.8% overall increase) in bin A and bin B (Figure 5F, 16.5% increase in bin A
251 and 11.8% increase in bin B). Interestingly, in mice, Pax6-Eomes+ IPs, which are the vast majority of endogenous
252 BPs of lissencephalic species[19], were significantly decreased after ZBTB16 overexpression (Figure 5E,F, 10.6%
253 decrease in bin A and 15.1% decrease in bin B). In addition, ZBTB16 seems to increase the self-renewing capacity
254 of the cells it is overexpressed in as we observed a significant increase of BRDU+Ki67+ cells in bins A and B
255 compared to control electroporations (cell cycle re-entry analysis with BRDU for 24 hours, Figure S9, see
256 Supplemental Results for more details). Our results thus suggest that ZBTB16 overexpression in lissencephalic
257 neurogenesis leads to increased gyrified species-enriched BPs at the expense of the endogenous neurogenic
258 progenitors.
259 To further study what this means for neurogenesis we analyzed the neuronal output. Here, we found that ZBTB16
260 overexpression led to increased numbers of layer V neurons expressing Bcl11b (33.3% significant increase, Figure
261 5G,H) and layer VI neurons expressing Tbr1 (4.3% significant increase, Figure 5G,I) but not of upper layer IV
262 neurons that express Satb2 (Figure S10C,D). Given that in mice it is known that upper layer neurons are mainly

263 born starting at E14.5 and not before[32], we repeated the same experiments but performing the IUEs a day later, at
264 E14.5, and analyzing neuronal output at E17.5. Indeed, at this developmental stage ZBTB16 overexpression leads
265 to increased numbers of Satb2+ cells compared to the control plasmid (14% significant increase, Figure S10F,G).
266 We also still find increased numbers of Bcl11b+ cells (26% significant increase, Figure S10G). Thus, in mice
267 ZBTB16-overexpression leads to increased numbers of both deep- and upper- layer neurons whereas in hCOs the
268 main effect of both dex and ZBTB16-overexpression is on upper-layer neurons, potentially highlighting differences
269 in the plasticity of these cells in a gyrified- or lissencephalic- context. When examining the distribution of neurons,
270 we found an accumulation in the SVZ- and IZ- areas with less neurons having reached the CP after ZBTB16
271 overexpression (Figure S10A,B,E). This finding again lends support to the fact that the higher proliferative capacity
272 of the PAX6+EOMES+ BPs associates with a potentially longer neurogenic period similar to what we observed
273 following dex treatment in hCOs. In fact, when analyzing the distribution of neurons across the five bins not 3 but 6
274 days post electroporation (i.e. at day E19.5/birth) there were no significant differences for the distribution of GFP+
275 cells with ZBTB16 overexpression (Figure S10H-L), indicating that migratory processes are probably not affected.
276
277 ***ZBTB16* directly induces *PAX6* expression**
278 Considering that dex via *ZBTB16* seems to sustain *PAX6* expression in EOMES+ cells, even in a lissencephalic
279 species where physiologically they are mutually exclusive[33–35], and that *ZBTB16* is a TF, we analysed the activator
280 capacity of ZBTB16 on *PAX6* human promoters. *PAX6* has three promoter regions that regulate tissue-specific
281 expression and that are highly conserved between humans and rodents: the P0, P1 and Pa promoters [36,37] (Figure
282 S11A). Using luciferase assays, we found that ZBTB16 activates the P1 promoter of *PAX6* but not the P0 and Pa
283 promoters (Figure S11B). This suggests that ZBTB16 could regulate *PAX6* expression via the P1 promoter which
284 is active during neocortical development, in comparison to the P0 and Pa promoters which are minimally active[36].
285 This could be a potential mechanism responsible for sustaining *Pax6* expression in Eomes+ cells even in mice by
286 ZBTB16 overexpression circumventing the negative feedback loop that physiologically ensures that *Pax6* and
287 *Eomes* are not co-expressed in rodents[33–35].
288
289 **Glucocorticoids interact with the *ZBTB16* genetic and epigenetic landscape**
290 In order to analyse the mechanisms via which the physiological temporal expression pattern of *ZBTB16* is affected
291 by GCs, we looked at the gene regulatory landscape of the human *ZBTB16* locus in response to GCs. ENCODE
292 data indicate the existence of intronic GR-response elements (GREs) at the human *ZBTB16* locus (Figure 6A). We
293 have previously shown that activation of GR leads to DNA methylation changes in GREs of target genes which
294 associates with changes in gene transcription[38,39]. To identify the molecular mechanism by which dex via GR
295 induced *ZBTB16* expression, we treated day 30 hCOs with 100nM dex for 7 days and used HAM-TBS[40] (Highly
296 Accurate Method for Targeted Bisulfite Sequencing) and Pyrosequencing to measure DNA methylation of all GREs,
297 as identified by public GR-ChIP sequencing datasets (Table S9) and additional non-GR-related regulatory elements
298 (Figure 6A). Out of 55 CpGs covered with HAM-TBS and 8 covered with Pyrosequencing, 44 were located within
299 GREs and 19 in enhancer elements lacking GR binding sites. While only 1 of the CpGs outside these GR-binding
300 regions showed significant DNA methylation level changes following dex stimulation (Table S10), this was true for
301 18 of the 44 CpGs around GREs (Figure 6B and Table S10). All significantly altered GRE-CpGs are located in
302 enhancer regions that loop to the transcriptional start site of *ZBTB16* ("GeneHancer" track in Figure 6A and Bothe
303 *et al.*, Life Science Alliance, 2021[41]). Our data thus support a model in which GR binds to these enhancer elements
304 as evidenced by altered DNA methylation and increases *ZBTB16* transcription.
305 Knowing that environmental factors, including GCs, can interact with the genetic landscape to modulate their effects
306 on expression[42], we next analyzed the genetic landscape of *ZBTB16*. We catalogued the SNPs (single nucleotide

307 polymorphisms) in the *ZBTB16* locus previously associated with neurobehavioral and brain structural outcomes
308 (GWAS Catalogue & Table S11) and identified rs648044 as the only variant associated with both (Table S12).
309 rs648044 has been associated with educational attainment in two GWAS (genome-wide association study) for this
310 trait (Lee *et al.*[43]: N= 1,131,881, FDR = $9*10^{-9}$ & Okbay *et al.*[44]: N= 3,037,499, FDR = $2*10^{-8}$) and with generalized
311 cortical thickness[45] (N= 35,657 individuals, FDR = $6*10^{-9}$). In the latter GWAS on cortical morphology, gene-level
312 analysis also identified the whole *ZBTB16* locus to be significantly associated with generalized cortical surface area
313 (FDR = $7.2*10^{-14}$) and thickness (FDR = $1.9*10^{-8}$), thus suggesting relevance of *ZBTB16* for adult cortical
314 morphology.
315 In our DNA methylation assays, CpGs surrounding this SNP showed low methylation levels supporting its regulatory
316 activity (Figure S12A and Table S10). To further explore its role in gene regulation, we first analyzed whether this
317 SNP moderates dex-induced activity of the surrounding 200 bp (base pair) enhancer element using a STARR-
318 qPCR (Self Transcribing Active Regulatory Region- qPCR) approach. We identified that the sequence surrounding
319 rs648044 indeed possesses enhancer activity that is increased with GR activation via dex (Figure S12B). The extent
320 of the dex-induced activity increase was rs648044 allele-dependent, with the allele associated with higher
321 educational attainment (A-allele), conferring a significantly stronger increase following dex (Figure S12C). Next, we
322 used CRISPR-Cas9 to KO 400 nucleotides surrounding rs648044 in No.1- iPSCs in order to identify whether this
323 enhancer affects *ZBTB16* transcription in hCOs. The rs648044 genotype of No.1- iPSCs is heterozygous (G/A),
324 with the rarer A allele (allele frequency = 0.35) creating a degenerated partial GR binding site (described half site[46]:
325 AGXACAG, rs648044 creates: AGC<u>A</u>GAG, Figure S12D). A KO of the A allele resulted in $rs648044^{G/-}$ cells that
326 only carry the G allele (Figure S12D). Using the edited cell line ($rs648044^{G/-}$) and the control cell line carrying both
327 alleles ($rs648044^{G/A}$), we found that the absence of the A allele confers significantly less induction of *ZBTB16*
328 following 100nM dex in day 30 hCOs treated for 7 days (Figure S12E), suggesting that the enhancer containing
329 rs648044 modulates dex-mediated transcriptional effects on *ZBTB16* in hCOs.
330
331 **Glucocorticoids x rs648044 effects on *ZBTB16* relate to beneficial postnatal outcomes**
332 Given the functional effects of rs648044 on GC-induced ZBTB16 expression in the developing cortex, we used
333 phenome-wide mendelian randomization analysis (MRa-PheWAS) to identify causal effects of *ZBTB16* levels on
334 7,323 phenotypes from the UK Biobank and the NHGRI-EBI GWAS Catalog (Table S13) that include, among many
335 others, neurobehavioral traits and adult neuroimaging data. We used rs648044 as exposure and the magnitude of
336 the allele-specific expression changes following dex in the STARR-qPCR experiment as instrument to test for these
337 associations. MRa-PheWAS provided strong evidence for associations with multiple outcomes as indicated by the
338 QQ-plot (Figure S12G). MRa on various phenotypes, including endophenotypes and diseases (N= 4,360), showed
339 significant associations of GC-altered *ZBTB16* expression with 22 phenotypes after multiple testing correction.
340 These included positive associations with years of schooling and whether individuals had obtained a college or
341 university degree (Figure 6C and Table S14), which are direct measures of educational attainment. This supports
342 the idea that the functional effects of rs648044 on GC-induced *ZBTB16* transcription in the developing cortex, are
343 putatively causally-related to educational attainment postnatally. In addition, GC-induced *ZBTB16* transcription was
344 negatively associated with “fed-up feelings” a phenotype related to neuroticism[47], “alcohol intake” and “time spent
345 watching television” (Figure 6C), suggesting associations of higher *ZBTB16* levels with beneficial postnatal
346 outcomes and decreased associations with negative outcomes. Given the previously published relationships of both
347 educational attainment[48–51] as well as rs648044[43–45] with cortical volumes and white matter measures, we also ran
348 an MRa-PheWAS on all neuroimaging phenotypes (N = 3,143) in the UK Biobank using the same instrument. We
349 observed 21 significant associations after multiple testing correction (Figure 6D, Figure S12H and Table S15). Most

350 evidence indicated that GCs x rs648044-mediated increases in *ZBTB16* expression were significantly associated
351 with altered white matter measures and with higher anterior circular insula thickness (Figure 6D).
352 To further examine the importance of GC-altered *ZBTB16* levels during neurogenesis for postnatal phenotypes, we
353 used data from the Intra-Uterine (ITU) sampling in early pregnancy prospective cohort study[52] to test the association
354 of the rs648044 A allele and cortisol with cognitive performance. The ITU cohort comprises of 944 mother-child
355 dyads. Neuropsychological assessment of the children was performed at 35.6 months of age (range 24.5 to 42.5)
356 using the Bayley-III screening test[53] designed to identify infants and toddlers at risk for developmental delay. We
357 defined neurodevelopmental cognitive delay, using the Bayley cognitive subscale, as one standard deviation (SD)
358 below the sample mean (Figure S12I). For children testing below and above 1 SD of cognitive performance, a
359 complete set of salivary cortisol data during pregnancy and fetal genotypes was available for 246 mother-child
360 dyads before GW28 and for 221 mother-child dyads after GW28 (Table S16). Using logistic regressions, we tested
361 the interaction of rs648044 A allele * mean cortisol levels before GW28, after GW28 or across pregnancy on
362 cognitive performance at 3 years of age (see Methods for covariates). The interaction was not significantly
363 associated with cognitive performance when using cortisol levels from across pregnancy (p-value 0.055, Table
364 S17). Interestingly, when stratifying the data for cortisol levels before GW28, and thus during neurogenesis, the
365 interaction of rs648044 A allele with cortisol was significantly associated with higher cognitive performance (p-value
366 0.035, Figure 6E, Table S17), an effect not found with cortisol data after GW28 (p-value = 0.46, Table S17) and
367 thus after the end of neurogenesis.
368 Thus, higher GC-induced *ZBTB16* expression in rs648044 A allele carriers during neurogenesis might drive the
369 association of GC treatment with higher cognitive performance, higher educational attainment, lower neuroticism
370 measures and increased cortical thickness as well as altered white matter measures postnatally. This suggests that
371 the genetic association of this variant with postnatal and adult neurobehavioral and brain structural measures could
372 be mediated in parts by its effects on GC-induced *ZBTB16* levels in early brain development and in consequence
373 their effects on neurogenesis.
374
375 **Discussion**
376 With this work we sought to understand the effects of GCs during human cortical neurogenesis at the cellular and
377 molecular levels. Our results provide a novel molecular and cellular mechanism for GC effects on neurogenic
378 processes and also directly relate it to neurobehavioral, cognitive and brain structural outcomes after birth. We
379 found that GCs increase a particular population of neural progenitor cells that co-express PAX6 and EOMES. These
380 progenitor cells were found at the basal side of the germinal zones and are known to be enriched in species with
381 gyrified brains and related to a higher proliferative capacity, contributing to increased neuronal production[19,20,54].
382 Indeed, we found these BPs to have higher self-renewing capacity while neurogenesis was also increased. We
383 show that these effects of GCs are mediated by an alteration of the developmental expression profile of a TF called
384 *ZBTB16*. *ZBTB16* activates a forebrain active promoter of *PAX6*, potentially explaining how GCs increase the
385 numbers of PAX6+EOMES+ BPs. The increase in these specific BPs is followed by increased numbers of neurons,
386 albeit cell lineage experiments would be needed to directly prove the association, and relates to beneficial postnatal
387 outcomes at the neurobehavioral level, like increased cognitive performance, educational attainment and altered
388 brain structure (Figure 6F).
389 Precise temporal and spatial regulation of gene expression by TFs is key for the proper unfolding of neurogenic
390 processes[25]. Thus, we focused on GC-effects on TFs as the potential molecular mechanism responsible for their
391 effects on neurogenesis. We showed that GCs alter the tightly regulated developmental expression profile of a TF
392 called *ZBTB16* in hCOs which in turn mediates the GC-effects on neurogenesis. While ZBTB16 shows a dynamic
393 expression pattern in both gyrencephalic and lissencephalic species, the expression among species differs

394 according to developmental time-windows. In mice, *Zbtb16* appears at E7.5 in the neuroectoderm, increases until
395 E10.5 and is subsequently downregulated and finally only expressed in specific areas of the hindbrain and the
396 septum but not the forebrain[28], so that in rodents *Zbtb16* is not expressed during cortical neurogenesis. This is
397 contrary to the expression pattern observed in human fetal brain and hCOs (Figure S4), where *ZBTB16* is expressed
398 during the initial stages of neurogenesis. This points to possible divergent actions of this TF in gyrencephalic and
399 lissencephalic species neurodevelopment and highlights this protein as important for gyrified-species enriched
400 neurogenic processes at baseline as well as in response to GCs.
401 Indeed, overexpressing ZBTB16 in the mouse fetal brain during the neurogenic period (E13-E16, when *Zbtb16* is
402 not anymore expressed physiologically) leads to increased Pax6+Eomes+ BPs. In lissencephalic cortical
403 development *Pax6* and *Eomes* create a positive feedforward cascade that self-regulates with direct negative
404 feedback effects[33–35], ensuring mutually exclusive expression of these proteins. This seems to be overridden by
405 asynchronous overexpression of *ZBTB16*. We also show that *ZBTB16* directly activates the *PAX6* promoter P1[36],
406 that is functional in the forebrain, and sustains PAX6 expression potentially leading to the increased
407 PAX6+EOMES+ BPs both in hCOs and in mice. Thus, via the action of *ZBTB16,* GCs have the ability to extend or
408 open a sensitive developmental time-window for the production of gyrencephalic-enriched BPs in a lissencephalic
409 species resulting in enhanced neurogenic potential and higher production of neurons. *ZBTB16* seems to specifically
410 mediate the effects of GCs on neurogenesis since it is differentially regulated only in the progenitor clusters. Thus,
411 it is unlikely that it would mediate other reported in the literature GC effects that are specific to neuronal function,
412 as, for example, synaptic plasticity[55,56].
413 Given the high prevalence of premature births, GC excess during human neurodevelopment through administration
414 of sGCs is a very common phenomenon[9]. In fact, in about ~615,000 extreme preterm pregnancies per year, sGC
415 treatments, if used, would take place in a period of active neurogenesis, before GW28[10,16]. In fact, it was recently
416 shown that sGCs at GW22 increase the survival rate of the offspring 3.5 times, with the authors further supporting
417 and suggesting the use of SGCs in extremely premature births[11]. While endogenous GCs are important for the
418 maturation and function of fetal organs[4], prenatal excess of GCs has been extensively associated with long-term
419 metabolic, endocrine and cardiovascular problems[2] and risk for neurodevelopmental[57] and mental[58] disorders in the
420 offspring. Evidence from a recent meta-analysis of studies including more than 1,25 million children re-affirms the
421 association of exposure to sGCs with negative effects on cognitive and neuropsychiatric outcomes when
422 administered to children with late-preterm or term birth. However, the authors also report a significantly lower risk
423 for neurodevelopmental impairments in children with extremely preterm birth (< GW28), that were treated with sGCs
424 between GW22 to GW27[14]. This meta-analysis could be pointing to potential differential effects of GCs on
425 neurodevelopment depending on the developmental time-window they were administered in.
426 One process that is different among extremely preterm and term or adult brains and might contribute to these
427 dichotomous effects is human cortical neurogenesis, which peaks ~GW20 and is reduced but present until GW28
428 in the SVZ of the brain[16]. This means that extremely preterm born children are still treated within the time window
429 of active cortical neurogenesis. Such differential effects are supported by a study in mice in which dex administration
430 during neurogenesis was associated with anxiolytic and anti-depressive like behavior in the adult offspring[59] while
431 increased, prolonged exposure to GCs following completion of cortical neurogenesis has repeatedly been
432 associated with increased anxiety and depressive-like behaviors and decreased cognitive ability in these animals[60].
433 With this work we highlight a potential molecular and cellular pathway for the lasting effects of prenatal sGC
434 exposure during neurogenesis and pinpoint *ZBTB16* as an important hub gene mediating GC effect on cortical
435 neurogenesis and beneficial postnatal phenotypes. The latter is, on the one hand, supported by our results using
436 the ITU cohort where we find that that in carriers of the high *ZBTB16*-induction rs648044 allele, increased maternal
437 cortisol levels were associated with better cognitive performance, but only when considering cortisol levels before

GW28, i.e. during active neurogenesis, and not at later time points. It is additionally supported from the MRa-PheWAS where we find associations with higher educational attainment, lower neuroticism measures and altered cortical and white matter measures. Nevertheless, the association with postnatal behavioral and structural outcomes should be interpreted with caution as the increased number of neurons may ultimately not contribute to brain function postnatally.

Overall, our work provides a molecular and cellular mechanism of how GCs early in development, during the neurogenic period, affect the cytoarchitecture of the developing cortex which in turn associates with postnatal outcomes at the brain structural but also neurobehavioral level. This work highlights the importance of GCs for neurogenic processes in humans. In addition, the new knowledge offers a possible molecular and cellular pathway explaining the associations of early sGC use with beneficial behavioral and neurodevelopmental measures found in the literature and, thus, may help to refine sGC treatment guidelines according to the stage of pregnancy they are administered in.

**Acknowledgments**

LD acknowledges support by the Joachim Herz Foundation. We thank Mira Erhart, dr. Michael Czisch and dr. Benoit Boulat for informative discussions on the brain structural measures. We thank Nathalie Gerstner and dr. Janine Knauer-Arloth for discussion on data analysis. We thank dr. Nadine Gogolla for discussion on broader relevance of the findings. This work was supported by the Hope for Depression Research foundation and a NARSAD Distinguished Investigator award to EBB.

**Conflict of interest**

The authors declare no conflict of interest.

**Authors' contributions**

ACK conceived the idea, designed and carried out experiments, performed analyses, provided critical intellectual input, generated and revised the paper draft; CC designed and performed omics experiments, provided critical intellectual input and revised the paper draft; CK designed and performed electroporation experiments, provided critical intellectual input and revised the paper draft; LD performed analysis and revised the paper draft; MHL & CR performed cell biology experiments; NK & DP performed the phenome wide mendelian randomization analysis and revised the paper draft; SPG designed and provided critical intellectual input for the STARR experiments; AS, DC, MLP, SS, EW, KH and KR worked on creating and analysing the ITU cohort, provided data and analysis pipelines; SR performed analysis and revised the paper draft; VS, BW, MK & SS performed experiments; MRH supported project organization and experimental procedures; ML designed and performed CRISPR-Cas9 experiments, provided critical intellectual input and revised the paper draft; SC provided critical intellectual input and revised the paper draft; EBB conceived the idea, obtained funding, supervised the study, designed experiments and analysis pipelines, provided critical intellectual input and contributed to paper draft writing and revisions.

**Supplemental Information**

Supplemental Results

Supplemental Tables 1-21

Supplemental Figures 1-12

**Figures**

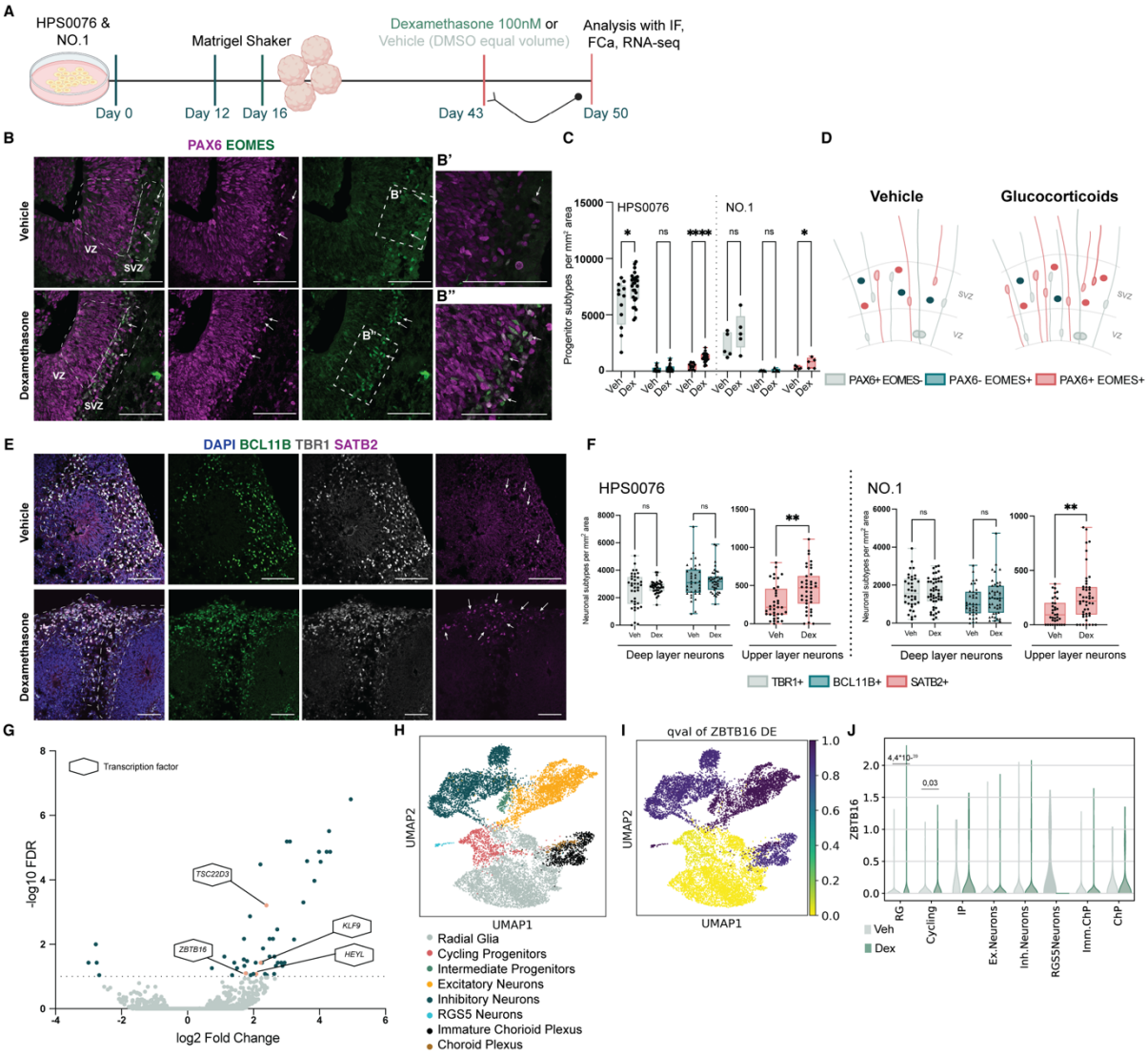


**Figure 1l Glucocorticoids increase basal progenitors that co-express PAX6 and EOMES. A,** Treatment and analysis workflow in human cerebral organoids (hCOs) derived from two iPSC lines. **B,** Representative images of day 50 hCOs at veh and dex conditions stained for PAX6 and EOMES. Arrows indicate cells that co-express PAX6 and EOMES; Scale bars, 100µm. **B' and B'',** Zoom-ins of the areas shown in vehicle and dex ventricles respectively in Figure B. Scale bars, 100µm. **C,** Quantification of the progenitor subtypes in each treatment condition normalized by mm² of quantified total area in hCOs produced from two iPSC lines. **D**, Schematic representation of the effects of dex on progenitors, highlighting the increased numbers of basal progenitors co-expressing PAX6 and EOMES. **E,** Representative images of day 50 hCOs at vehicle and dex conditions stained for layer VI neurons with TBR1, layer V neurons with BCL11B, layer IV neurons with SATB2 and DAPI. Arrows indicate SATB2 positive cells in the CP; Scale bars, 100µm. **F,** Quantification of TBR1, BCL11B and SATB2 cells found in the CP normalized per mm² of area. **G,** Volcano plot of DE gene expression analysis in bulk RNA sequencing. Grey dots, genes with non-significant expression changes at an FDR cutoff of 10%; Blue dots, genes with significant expression changes; Orange dots denote TFs labeled with their gene name. **H,** Single-cell clusters of HPS0076 hCOs treated with dex 100nM for 10 days starting at day 60. **I,** UMAP plot showing *ZBTB16* FDR-value of dex response per cluster. **J,** Violin plot of *ZBTB16* expression changes per cluster. FDR, false discovery rate with Benjamini-Hochberg correction. DMSO, dimethyl sulfoxide; IF, Immunofluorescence; Seq, sequencing; Veh, vehicle; Dex, dexamethasone; VZ, ventricular-like zone; SVZ, subventricular-like zone; BPs, basal progenitors; CP, cortical plate; TFs, transcription factors; RG, Radial Glia; Cycling, Cycling Progenitors; IP, Intermediate Progenitors; Ex. Neurons,

Excitatory Neurons; Inh. Neurons, Inhibitory Neurons; Imm. ChP, Immature Choroid Plexus; ChP, Choroid Plexus. Significance was tested with two tailed Mann-Whitney comparison between treatment and vehicle. P-values: **** <=0.0001, ** <=0.01, * <=0.05, ns >0.05

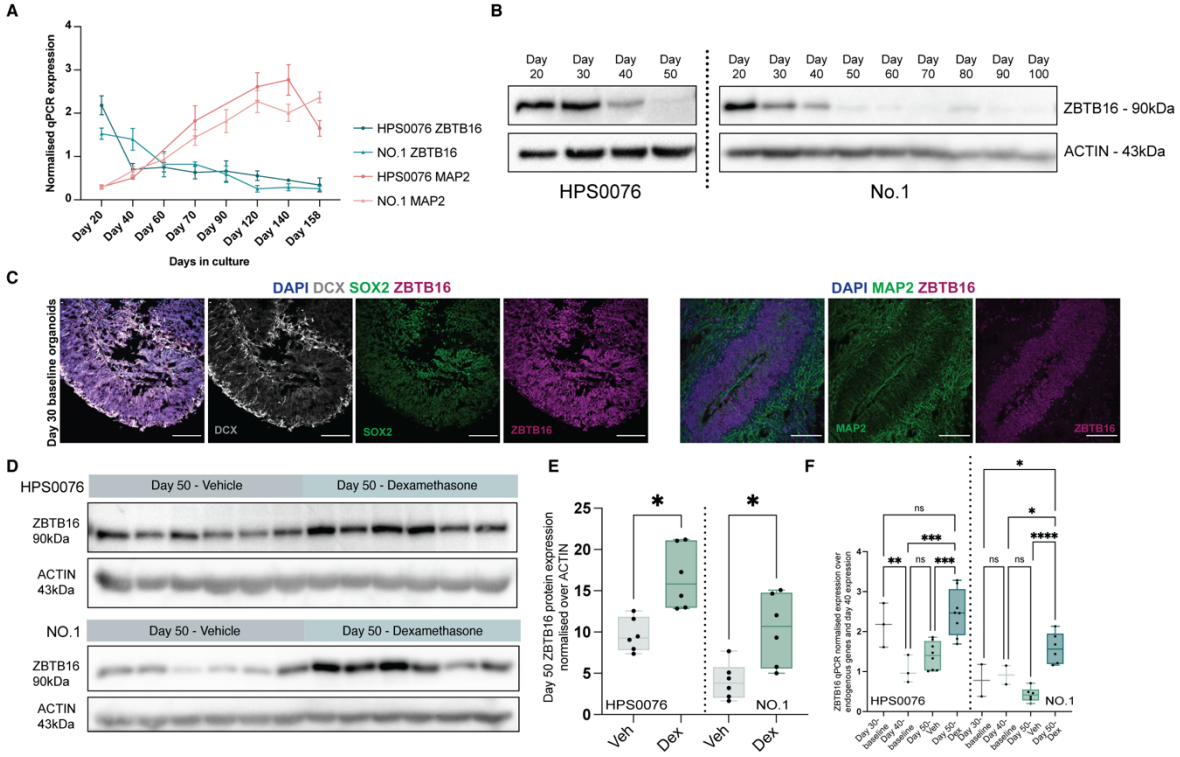


**Figure 2l Glucocorticoids alter the expression profile of *ZBTB16*. A,** qPCR results (mean +/- SEM) for ZBTB16 and MAP2 in hCOs of different developmental stages. **B,** Western blots of ZBTB16 and ACTIN proteins in hCOs of different developmental stages. **C,** Representative images of day 30 baseline hCOs stained for the immature neuron marker DCX, the progenitor marker SOX2, the mature neuronal marker MAP2, ZBTB16 and the nuclear marker DAPI Scale bars, 100µm. **D,** Western blots of ZBTB16 and ACTIN proteins in hCOs treated with 100nM of dex at day 43 and analysed 7 days later at day 50. Each lane contains protein from a pool of 3 organoids and the 6 replicates were generated in two independent hCOs batches, thus showing protein of 18 organoids from two independene batches in each treatment paradigm. **E**, Quantification of the effect of 100nM 7 days dex treatment on ZBTB16 protein expression in day 50 hCOs normalized over ACTIN. **F,** qPCR plot for ZBTB16 mRNA expression in hCOs and expression at days 30-50, with vehicle and dex condition at day 50. qPCR, quantitative polymerase chain reaction; hCOs, human cerebral organoids; Veh, vehicle; Dex, dexamethasone. For **E** significance was tested with two tailed Mann-Whitney comparison between treatment and vehicle. For **F** significance was tested with one-way ANOVA with Benjamini, Krieger and Yekutieli multiple testing correction (p= 0.0003, F= 10.39, DF= 3). Mann-Whitney p-values for E or post-hoc p-values for F: **** <=0.0001, *** <=0.001, ** <=0.01, * <=0.05, ns >0.05

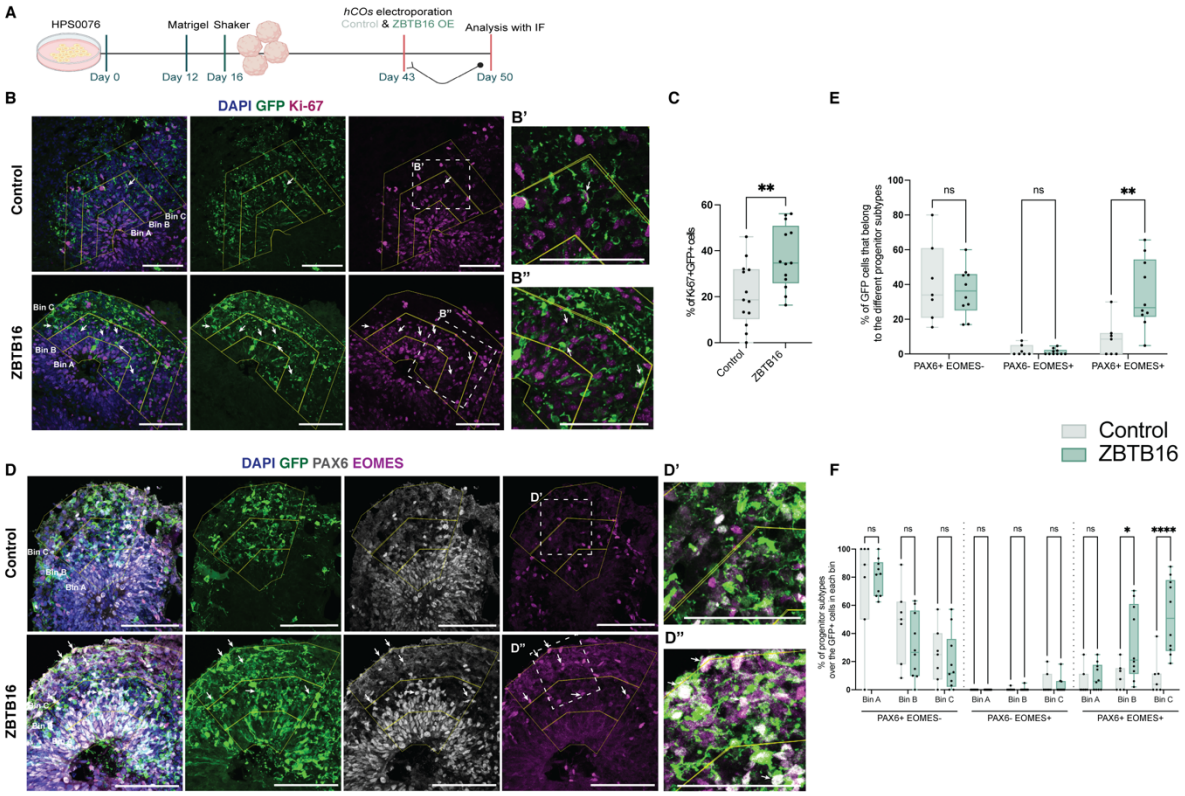


**Figure 3l *ZBTB16* increases PAX6+EOMES+ basal progenitors in human cerebral organoids. A,** Schematic of HPS0076-derived hCOs electroporations and analysis workflow for ZBTB16 OE. **B,** Representative images of day 50 hCOs at control and ZBTB16 OE conditions stained for Ki-67, GFP and DAPI. White arrows indicate GFP cells that express Ki-67; Scale bars, 100µm. **C,** Quantification of the total number of GFP cells that are Ki-67 positive normalized over total GFP cells. **D,** Representative images of day 50 hCOs at control and ZBTB16 OE conditions stained for PAX6, EOMES, GFP and DAPI. Arrows indicate GFP cells that co-express PAX6 and EOMES; Scale bars, 100µm. **D' and D",** Zoom-ins of the areas shown in control and ZBTB16-overexpressing ventricles respectively in Figure D. Scale bars, 100µm. **E,** Quantification of the GFP cells belonging in each progenitor subtype normalized by total GFP cells. **F,** Quantification of the GFP cells belonging in the different single positive progenitor subtypes in each bin and condition normalized by total GFP cells of each bin. hCOs, human cerebral organoids; OE, overexpression; IF, Immunofluorescence. For **C** significance was tested with two tailed Mann-Whitney comparison between ZBTB16-overexpression and control plasmid. For **E&F** significance was tested with two-way ANOVA with Benjamini, Krieger and Yekutieli multiple testing correction (E: p.interaction= 0.0069, F= 5.5, DF= 2/ F: p.interaction = 0.0002, F= 4.17, DF= 8). Mann-Whitney p-values for C or post-hoc p-values for E&F: **** <=0.0001, ** <=0.01, * <=0.05, ns >0.05

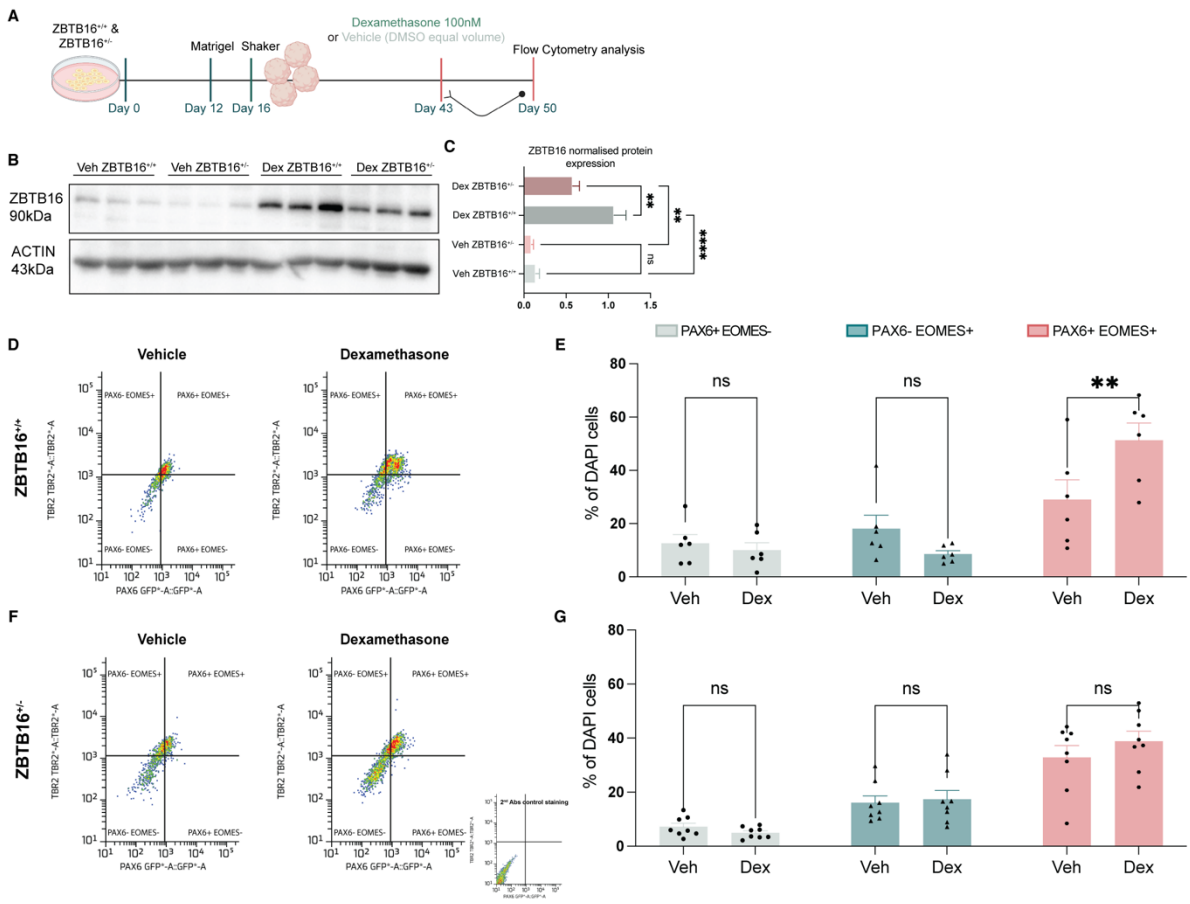


**Figure 4l *ZBTB16* mediates the effects of glucocorticoids on PAX6+EOMES+ basal progenitors. A,** Treatment paradigm and analysis workflow in hCOs derived from edited No.1- iPSCs either with ZBTB16$^{+/+}$ or ZBTB16$^{+/-}$ genotypes. **B,** Western blots for ZBTB16 and ACTIN proteins in ZBTB16$^{+/+}$ or ZBTB16$^{+/-}$ derived hCOs at different treatment conditions. Each lane contains protein from a pool of 3 organoids thus showing protein of 9 organoids in each treatment group and genetic background. **C,** Quantification of the Western blot results for ZBTB16 normalized over ACTIN. **D,** Representative images of FCa of ZBTB16$^{+/+}$-derived hCOs per dex treatment condition. TBR2 is an alternative name for EOMES. **E,** Quantification of the FCa results. Percentages of DAPI cells in each progenitor subtype and treatment condition. **F** Representative images of FCa analysis of ZBTB16$^{+/-}$-derived hCOs per treatment condition. **G,** Quantification of the FCa results. Percentages of DAPI cells in each progenitor subtype and treatment condition. DMSO, dimethyl sulfoxide; hCOs, human cerebral organoids; Veh, vehicle; Dex, dexamethasone; FCa, flow cytometry analysis. For **C,E&G** significance was tested with two-way ANOVA with Benjamini, Krieger and Yekutieli multiple testing correction (C: p.interaction = 0.03, F= 6.6, DF= 1/ E: p.interaction = 0.0068, F= 5.9, DF= 2/ G: p.interaction = 0.97, F= 0.38, DF= 2). Post-hoc p-values: ** <=0.01, ns >0.05

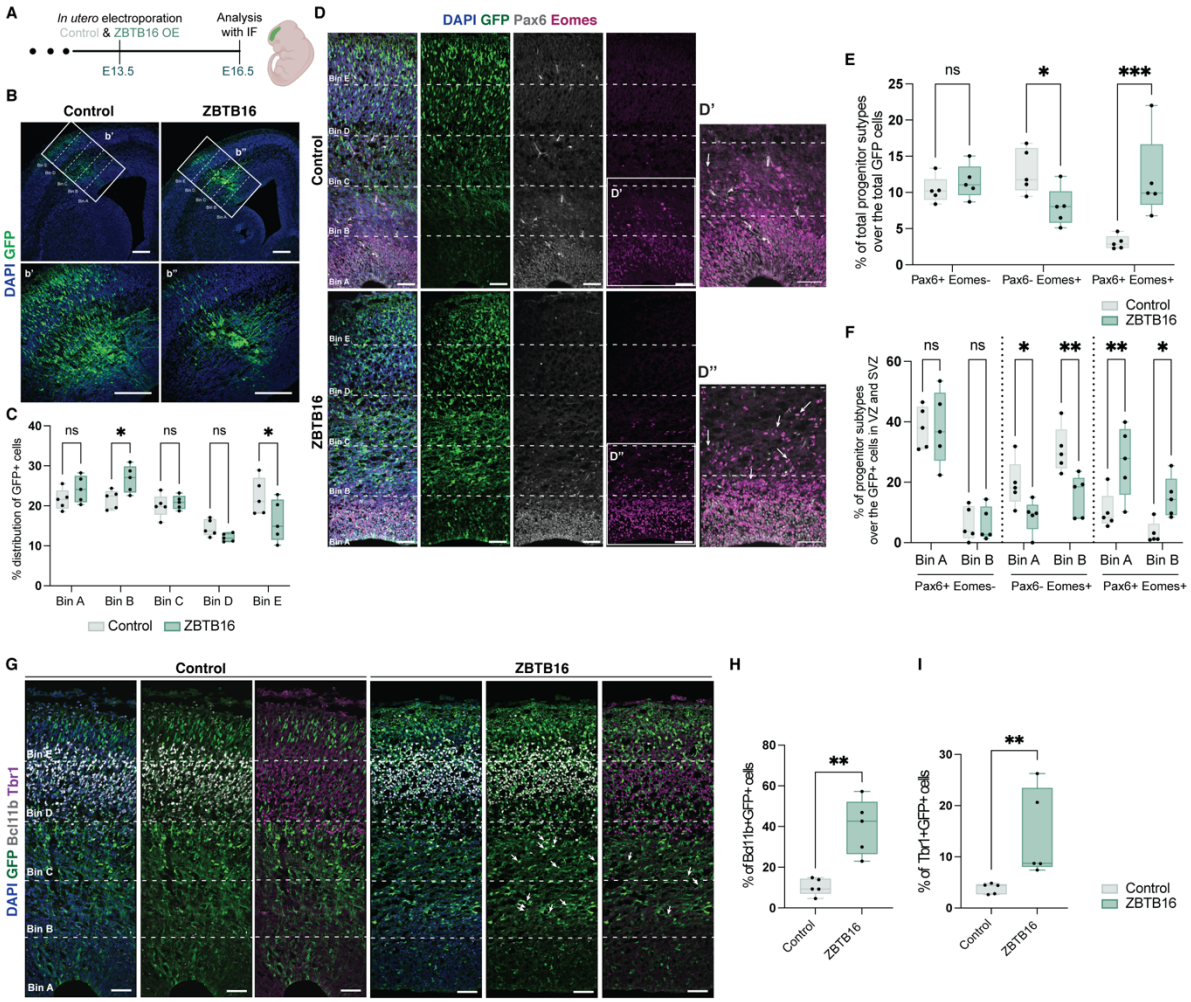


**Figure 5l *ZBTB16* increases PAX6+EOMES+ basal progenitors and deep layer neurons in a lissencephalic species. A,** Workflow of the *in utero* electroporations of *ZBTB16* and analysis in fetal mice. **B,** Representative images of E16.5 fetal mouse brains at control and ZBTB16 OE conditions stained for GFP and DAPI. Box indicates the electroporation areas and **b', b''** are zoom-ins; Scale bars, 100µm. **C,** Quantification of the distribution of GFP cells in each bin normalized by the total number of GFP cells. **D,** Representative images of E16.5 fetal mouse brains at control and ZBTB16 OE conditions stained for Pax6, Eomes, GFP and DAPI. **d' and d''** are zoom-ins. Arrows indicate GFP cells that co-express Pax6 and Eomes; Scale bars, 50µm. **E,** Quantification of the GFP cells belonging in the different progenitor subtypes normalized by total GFP cells. **F,** Quantification of the GFP cells belonging in the different positive progenitor subtypes in each bin normalized by total GFP cells of each bin. **G,** Representative images of E16.5 fetal mouse brains at control and ZBTB16 OE conditions stained for the layer V neuronal marker Bcl11b, layer VI neuronal marker Tbr1, GFP and DAPI. Arrows indicate GFP cells that express Bcl11b or that express Tbr1; Scale bars, 50µm. **H,** Quantification of the GFP cells that are Bcl11b+ normalized by total GFP cells. **I,** Quantification of the GFP cells that are Tbr1+ normalized by total GFP cells. OE, overexpression; IF, Immunofluorescence. For **H & I** significance was tested with two tailed Mann-Whitney comparison between ZBTB16-overexpression and control plasmid. For **C, E & F** significance was tested with two-way ANOVA with Benjamini, Krieger and Yekutieli multiple testing correction (C: p.interaction = 0.003, F= 4.7, DF= 4/ E: p.interaction = 0.0003, F= 11.84, DF= 2/ F: p.interaction < 0.0001, F= 6.58, DF= 5). Mann-Whitney p-values for H or post-hoc p-values for C,E &F: *** <=0.001, ** <=0.01, * <=0.05, ns >0.05

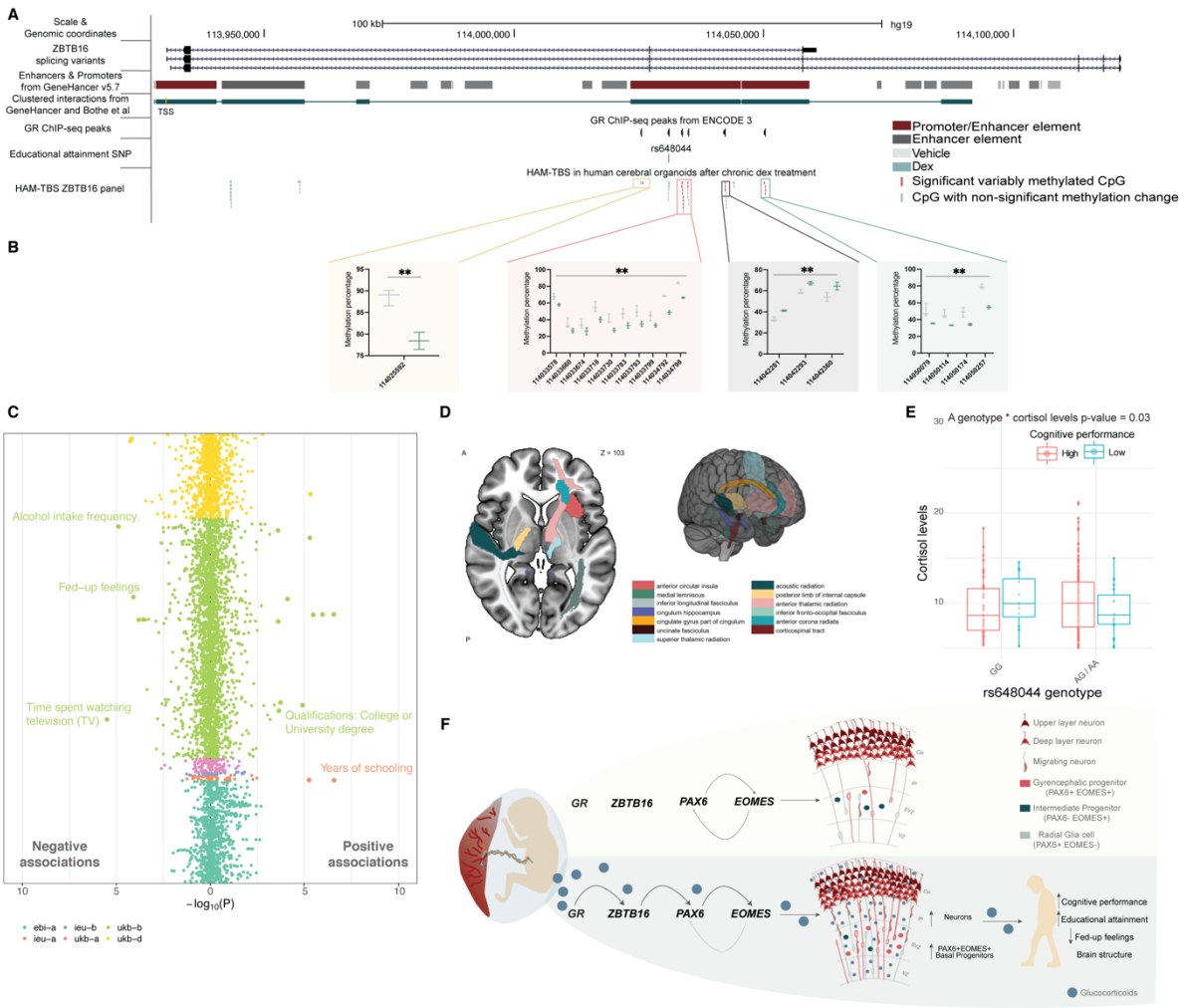


**Figure 6l Glucocorticoids interact with the genetic and epigenetic landscape of ZBTB16 to impact postnatal neurobehavioral and structural phenotypes. A,** Graphical representation of the ZBTB16 locus including the position of the amplicon for HAM-TBS and Pyrosequencing. **B,** HAM-TBS results for CpGs with significantly altered DNA methylation levels following exposure to 7 days of 100nM dex vs. vehicle. **C,** Plot depicting Phe-WAS-MRa associations as -log of the p-value for rs648044 with various phenotypes from the UK Biobank. Single phenotypes are depicted as individual points. Associations are presented based on negative (negative MRa estimate.i.e. lower quantitative measures with A-allele effects) and positive (positive MRa estimate, i.e. higher quantitative measures with A-allele effects) effects. Color coding reflects the different sources of GWAS depicted in the legend. Traits that remain significant following Benjamini-Hochberg correction are shown with larger dots and are listed in Table S14. All neurobehavioral traits are labeled. **D,** Illustration of significant MRa associations between brain imaging phenotypes and rs648044 mapped onto the brain atlases. All effects are listed also in Table S15. **E,** Cortisol levels before GW28 according to rs648044 genotype and cognitive performance as assessed using the Bayley-III cognitive subscale in the data from the ITU cohort. Total cortisol output was estimated based on the area under the curve with respect to ground (AUCg) of all seven saliva samples using the trapezoid rule in 246 mothers. **F,** Summary of the effects of glucocorticoids on ZBTB16 expression, cortical cellular architecture during development and postnatal phenotypes. GR, glucocorticoid receptor; ChIP, chromatin immunoprecipitation; Seq, sequencing; SNP, single nucleotide polymorphism; HAM-TBS, highly accurate method for targeted bisulfite sequencing; Dex, dexamethasone; MRa, mendelian randomization analysis. For **B** significance was tested with two-way ANOVA with

592 Benjamini, Krieger and Yekutieli multiple testing correction (GH11J114152 enhancer: p.treatment < 0.0001, F=
593 7.33, DF= 31/ GH11J114174 enhancer: p.treatment< 0.0001, F= 37.32, DF= 3). Post-hoc p-values: ** <=0.01

594

595 **STAR Methods**

596 **Resource availability**

597 Lead contact

598 Further information and requests for resources and reagents should be directed to and will be fulfilled by the lead
599 contact, Elisabeth Binder (binder@psych.mpg.de).
600

601 Materials availability

602 Plasmids generated in this study are available upon request.

603 Human iPSC lines used in this study are subject to MTA approvals.

604

605 Data and code availability

606 Scripts and data for the MRa-PheWAS analyses are openly available via https://osf.io/4ud6q/ for full transparency.

607 Data for the bulk RNA-seq are deposited as BioProject under accession code PRJNA865917.
608

609 **Method details**

610 iPSCs

611 HPS0076 Human induced pluripotent stem cells (hiPSCs) were obtained from the RIKEN BRC cell bank and
612 reprogrammed from skin fibroblasts of a female donor (HPS0076- 409b2)[61,62]. No.1 hiPSCs were reprogrammed
613 from NuFF3-RQ newborn foreskin feeder fibroblasts of a male donor (GSC-3404, GlobalStem)[63]. MTA approvals
614 were obtained for the use of both hiPSC lines. hiPSCs were cultured in Matrigel-coated (1:100 diluted in DMEM-
615 F12 (Gibco™, 31330-038), Corning Incorporated, 354277) Costar® 6-well cell culture plates (Corning Incorporated,
616 3516) in mTESR1 Basal Medium (STEMCELL Technologies, 85851) supplemented with 1x mTESR1 Supplement
617 (STEMCELL Technologies, 85852) at 37°C with 5% $CO_2$. Passaging was performed with Gentle Cell Dissociation
618 Reagent (STEMCELL Technologies, 07174). RevitaCell Supplement (1:100 diluted, Gibco™, A2644501) was added
619 the day of the dissociation for 24 h to increase cell survival.
620

621 Cerebral organoids

622 Human cerebral organoids (hCOs) were created as previously described by Lancaster *et al*[17] with some
623 modifications. Briefly, hiPSCs were dissociated in StemPro Accutase Cell Dissociation Reagent (Life Technologies,
624 A1110501). Nine thousand single cells were plated into Ultra-low attachment 96-well plate round bottom wells
625 (Corning Incorporated, 7007) in human embryonic stem cell medium (hESC, DMEM/F12-GlutaMAX (Gibco™,
626 31331-028) with 20% Knockout Serum Replacement (Gibco™, 10828-028), 3% FBS (Fetal Bovine Serum, Gibco™,
627 16141-061), 1% non-essential amino acids (Gibco™, 11140-035), 0.1 mM 2-mercaptoethanol (Gibco™, 31350-010))
628 supplemented with 4 ng/ml human recombinant FGF (Fibroblast Growth Factor, Peprotech, 100-18B) and 50 μM
629 Rock inhibitor Y27632 (Millipore, SCM075) for 4 days and in hESC medium without bFGF and Rock inhibitor for an
630 additional 2 days to form embryoid bodies (EBs). On day 6, the medium was changed to neural induction medium
631 (NIM, DMEM/F12 GlutaMAX supplemented with 1:100 N2 supplement (Gibco™, 15502-048), 1% Non-essential
632 amino acids and 1 μg/ml Heparin (Sigma, H3149)) and cultured for an additional 6 days. On day 12, the EBs were
633 embedded in Matrigel (Corning Incorporated, 354234) drops and transferred to 10-cm cell culture plates (TPP,
634 93100) in neural differentiation medium without vitamin-A (NDM-A, DMEM/F12GlutaMAX and Neurobasal (Gibco™,
635 21103-049) in ratio 1:1 supplemented with 1:100 N2 supplement 1:100 B27 without Vitamin A (Gibco™, 12587-010),

636 0.5% non-essential amino acids, insulin 2.5 μg/ml (Gibco™, 19278), 1:100 Antibiotic-Antimycotic (Gibco™, 15240-
637 062) and 50 μM 2-mercaptoethanol) for 4 days. On day 16, hCOs were transferred onto an orbital shaker in NDM+A
638 medium (same composition as NDM-A with the addition of B27 with Vitamin A (Gibco™, 17504-044) in the place of
639 B27 without Vitamin A) and were grown in these conditions at 37°C with 5% $CO_2$. NDM+A medium was changed
640 twice per week.
641
642 Bulk RNA sequencing
643 RNA was isolated from day 45 No.1- hCOs in triplicates with 2-3 organoids pooled per replicate, either treated with
644 100nM dex for 7 days or veh (DMSO). Sequencing libraries were prepared using the QuantSeq 3' mRNA Fwd kit
645 (Lexogen) following manufacturer's instructions. Sequencing was performed on an Illumina HiSeq4000 sequencer
646 generating 150 bp long single-end reads. Read quality was verified using FastQC version 11.4[64]. For adapter
647 trimming and quality filtering the software cutadapt version 1.9.1[65] was used. For read alignment and gene
648 quantification salmon version 0.43.1[66] was applied setting the parameters noLengthCorrection and
649 perTranscriptPrior to account for the tag sequencing approach. Differential gene expression was assessed using
650 the R package DESeq2[67]. Data are openly available as BioProject with accession number PRJNA865917.
651
652 *In utero* electroporations of mice
653 All experiments and protocols were performed in accordance with the European Communities' Council Directive
654 2010/63/EU and were approved by the committee for the Care and Use of Laboratory Animals of the Government
655 of Upper Bavaria. All mice were obtained from the in-house breeding facility of the Max Planck Institute of Psychiatry
656 and kept in group housed conditions in individually ventilated cages (IVC; 30cm x 16 cm x 16 cm; 501 cm2) serviced
657 by a central airflow system (Tecniplast, IVC Green Line – GM500). Animals had ad libitum access to water (tap
658 water) and standard chow and were maintained under constant environmental conditions (12:12 hr light/dark cycle,
659 23 ± 2 °C and humidity of 55%). Time-pregnant female mice at stage E13.5 or E14.5 were anesthetized by
660 intraperitoneal injection of saline solution containing fentanyl (0.05 mg per kg body weight), midazolam (5 mg per
661 kg body weight), and medetomidine (0.5 mg per kg body weight) and embryos were electroporated as described in
662 Nature Protocols by Saito *et al* [68]. In brief, plasmids were mixed with Fast Green (2.5 mg/µL; Sigma F7252) and 1-
663 2μl were injected at a final concentration of 1μg/µL using glass micropipettes (5-000-1001-X10, Drummond
664 Scientific). The DNA was electroporated into the cells by delivering 5 pulses applied at 40V for 50ms in 1sec
665 intervals. Anesthesia was terminated by injection of buprenorphine (0.1 mg per kg body weight), atipamezole (2.5
666 mg per kg body weight), and flumazenil (0.5 mg per kg body weight). The pups remained *in utero* for 3 or 6 more
667 days, after which euthanizing occurred and the pups' brains were isolated. Brains were fixed at 6dpe (days post
668 electroporation) in 4% PFA (paraformaldehyde) for 16 h, cryo- preserved with 30% sucrose for at least 16 h and
669 stored at –20 °C in OCT (optimal cutting temperature, Thermo Fischer Scientific, 23-730-571). For
670 immunofluorescence, 12 μm cryosections were prepared on SuperFrost™ slides. For the cell cycle re-entry
671 experiment, embryos were electroporated at E13.5 and the mother received an intraperitoneal injection of 14mg/
672 100g of body weight of BRDU diluted in saline at E15.5, 24 hours before sacrifice at E16.5.
673
674 Electroporations of human cerebral organoids
675 HPS0076-hCOs were electroporated as described in[69,70]. In brief, hCOs were kept in antibiotic-free NDM+A medium
676 for three h prior to electroporation. Electroporation was performed in hCOs at day 43 after the initial plating of the
677 cells, and fixed at 7dpe. During electroporation, hCOs were placed in an electroporation chamber (Harvard
678 Apparatus, Holliston, MA, USA) under a stereoscope. Using a glass micropipette (5-000-1001-X10, Drummond
679 Scientific) 0.5 μL of plasmid DNA was injected together with Fast Green into different ventricles at a final

680 concentration of 1$\mu$g/µL. hCOs were subsequently electroporated with 5 pulses applied at 80 V for 50 ms each, at
681 500 ms intervals (ECM830, Harvard Apparatus). Following electroporation, hCOs were kept for an additional 24 h
682 in antibiotics-free NDM+A media and then changed into the normal NDM+A media until fixation at 7dpe. hCOs were
683 fixed using 4% PFA for 1 hour at 4 °C, cryo- preserved with 30% sucrose for 16 h and stored at –20 °C in OCT. For
684 immunofluorescence, 16 $\mu$m cryosections were prepared on SuperFrost™ slides.
685
686 Glucocorticoid treatment in cerebral organoids and mice
687 *hCOs*: Day 43 hCOs of both lines were treated for 7 days (chronic treatment) with 100nM of dexamethasone (dex).
688 To achieve the concentration used, dex was diluted in DMSO (dimethyl sulfoxide) in a concentration of 100µM and
689 subsequently diluted in NDM+A culture medium to a final concentration of 100nM. The DMSO control (vehicle- veh)
690 underwent the same dilutions as described for dex. The medium was changed every two days. At the end of the
691 treatment, hCOs were fixed using 4% PFA for 1 hour at 4 °C, cryo- preserved with 30% sucrose for 16 h and stored
692 at –20 °C in OCT. For immunofluorescence, 16 $\mu$m cryosections were prepared on SuperFrost™ slides.
693
694 *Fetal mice*: We injected fetal mouse brains at E13.5 (embryonic day 13.5) with dex diluted in DMSO and analysed
695 the effects at E16.5. To achieve ~100nM of dex concentration we measured the volume of E13.5 mouse brains by
696 measuring the volume displaced when submerged in saline, to ~25µl. Thus, we injected 1µl of 2.5µM dex or veh
697 into an E13.5 mouse brain ventricle to achieve a final concentration of ~100nM.
698
699 *Concentration and timing rationale:* The concentration of 100nM was chosen to mimic the antenatal corticosteroid
700 therapy scheme used during pregnancy. The guidelines for sGC use are four doses of 6mg dex every 12 h given
701 intramuscularly[8,71] when used in at risk for preterm birth pregnancies. A single dose of 6mg reaches a $C_{max}$ of 65-
702 95ng/µl at $T_{max}$ 3 h[71] which equals to a concentration of ~162nM-245nM, whereas 1.5mg would equal to ~40.4nM-
703 61.25nM. The maternal to fetal steroid hormones ratio has been reported anywhere from 0.4 and higher, days after
704 the treatment[71]. So, from a single 6mg dose we would expect at the very least ~64.8nM-98nM reaching the fetus
705 after 3 h post treatment. Similarly, from 1.5mg given each day we would expect at least ~16.16nM-39.2nM reaching
706 the fetus after 3 h post treatment. A previously published study that used 100nM of androgens, which are also
707 steroid hormones, in hCOs measured an actual concentration of 16nM[72]. They attributed this phenomenon to the
708 fact that steroid hormones have high affinity to plastic due to their lipophilic nature[73]. Since our primary aim was to
709 study the role of sGC therapy schema, the use 100nM of dex should parallel the amounts reaching the embryo by
710 the clinically used concentrations. As mentioned the schema of antenatal corticosteroids treatment is four doses
711 during a two-days' time. Dexamethasone is a long-acting corticosteroid with a biological half-life of 36 to 54/72
712 hours[74]. Considering the active administration time and the biological half-life of the steroid, we would expect dex
713 effects on the fetus for 5-7 days, with peak exposure for 2-3 days and then a decrease. Thus, we chose to administer
714 dex for 7 days.
715
716 Immunofluorescence
717 Sections were post-fixed in 4% PFA for 10 min at RT and permeabilized with 0.3% Triton in PBS for 5 min. Sections
718 were subsequently blocked with 0.1% TWEEN, 10% Fetal Bovine Serum and 3% BSA. Primary and secondary
719 antibodies (see Table S18) were diluted in blocking solution and nuclei were visualized using 0.5 $\mu$g/mL 4,6-
720 diamidino-2-phenylindole (DAPI, Sigma Aldrich). Cover slips were mounted with Aqua Poly/Mount (Polysciences,
721 18606-20). For PAX6, EOMES, BCL11B, ZBTB16, SOX2, Ki-67, TBR1 and SATB2 antigen retrieval was performed
722 before fixing with PFA. Briefly, sections were incubated with citric buffer (0.01 M, pH 6.0) for 1 min at 720 Watt and
723 10 min at 120 Watt, left to cool down at RT for 20 min and washed three times with PBS for 5 min.

724
725 Protein isolation and Western blot
726 Proteins were isolated on ice in RIPA buffer (Sigma-Aldrich, R0278) supplemented with protease (Sigma Aldrich,
727 P8340) and phosphatase inhibitors (Sigma Aldrich, 4906845001). For each experiment three biological replicates
728 were included each bearing the homogenate of three individual hCOs. 30$\mu$g of protein extracts were separated by
729 SDS-PAGE with an 8% gel. Proteins were transferred to a PVDF membrane (Millipore, IPVH00010). For detection,
730 membranes were incubated with primary antibodies (Table S18) for 16 h at 4$^{o}$C and with horse- radish peroxidase-
731 labeled secondary antibodies (Table S18) at RT for 1 hour. Subsequently, they were treated with Immobilon
732 Western HRP Substrate Luminol Reagent and Solution (Millipore, WBKLS0500) to visualize the bands. The
733 quantification was performed in the Bio-Rad Image Lab Software (Version 6.1). Relative protein expression levels
734 were quantified and normalized with ACTIN as endogenous control.
735
736 RNA isolation and quantitative PCR
737 Total RNA was extracted from hCOs using the RNeasy Mini extraction kit (Qiagen, 74104) according to the
738 manufacturer's instructions. For each experiment three biological replicates were included each bearing the
739 homogenate of three individual hCOs. Complementary DNA (cDNA) synthesis was performed using the Maxima H
740 Minus Reverse Transcriptase (Thermo Fisher, EP0751) with oligo(dT)16 primers (Invitrogen, N8080128) and
741 random hexamers (IDT DNA Technologies, 51-01-18-25) in a 1:1 ratio. Quantitative PCR (RT-qPCR) reactions
742 were run in quadruplicate using PrimeTime qPCR Primer Assays (IDT DNA Technologies, Table S19) and
743 PrimeTime® Gene Expression Master Mix (IDT DNA Technologies, 1055770) on a LightCycler 480 Instrument II
744 (Roche). Relative gene expression levels were quantified using the relative quantification method and normalized
745 with POLR2A and YWHAZ as endogenous control genes. Data shown are additionally normalized over the vehicle
746 samples so that vehicle samples have values of approximately one.
747 *Dexamethasone effects on fetal mice*: For the effect of dex on ZBTB16 transcription at least five different fetal
748 mouse brains were analyzed per condition. After brain isolation both cortices were excised, RNA was isolated and
749 quantitative PCR was performed as already described.
750
751 Plasmids preparation
752 Multiple PCR inserts were simultaneously cloned by In-Fusion HD Cloning Plus into the linearized vector pCAG-
753 DsRed2 (Addgene, #15777) to create the pCAG-ZBTB16-F2A-GFP plasmid. More specifically, the human ZBTB16
754 ORF (NM_006006.5, 2034bp) sequence was amplified from a plasmid delivered from GenScript and the F2A-GFP
755 from the Snap25-LSL-2A-GFP vector (Addgene, #61575). PCR primers were designed for the sequence of interest
756 with extensions that are complementary to the ends of the linearized vector or the corresponding fragment (Table
757 S19). PCR was performed using the CloneAmp HiFi PCR Premix (Takara Bio, 639298) following manufacturer's
758 instructions
759 After cloning the fragments for 3 h at 37$^{o}$C, the new construct was transformed into StellarTM competent cells and
760 grown for 16 h on agar plates containing 100µg/ml ampicillin. Single colonies were picked, plasmidic DNA was
761 isolated with Qiagen plasmid kits (12123, 12143) and the genotype was checked with Sanger sequencing (Table
762 S19). The pCAG-F2A-GFP plasmid was created by cutting the ZBTB16 fragment out of the pCAG-ZBTB16-F2A-
763 GFP plasmid using the BamhI and BglI restriction enzymes.
764
765 Luciferase reporter assays
766 Luciferase assays were designed to assess the activity of the three human *PAX6* promoters[75], P0, P1 and Pa (Table
767 S20) under ZBTB16 overexpression. The promoter sequences were cloned into the firefly luciferase (Luc2) reporter

768 expression pRP vector by VectorBuilder. The human ZBTB16 expression plasmid was generated by VectorBuilder
769 using the pRP backbone. 500ng of total plasmid DNA (75% of human ZBTB16 expression plasmid, 15% of reporter
770 plasmid and 10% of the pCAG-F2A-GFP, as internal control of transfection efficiency) were transfected into 72,000
771 HeLa cells in a well of a 24 well plate using Lipofectamine 2000 (ThermoFisher Scientific) following manufacturer's
772 instructions. All transfections were carried out in triplicates. HeLa cells were cultured in DMEM-F12 medium
773 (Gibco™, 11320033) supplemented with 10% FBS (Gibco™, 16141-061) and 1x Antibiotic-Antimycotic (Gibco™,
774 15240-062). The medium was refreshed the next day and 48 h later transfected cells were PBS washed and
775 incubated for 15 min at RT in 1x passive lysis buffer (Biotium, 99821). Plates were kept at least 1 hour at -80°C.
776 Next, the lysate was scraped and centrifuged at full speed for 30 sec at 4°C. 20µl of the supernatant was subjected
777 to the luciferase assay with the addition of 50 ul D-luciferine (Beetle Juice luciferase assay, PJK, 102511-1) by
778 using a Tristar multimode reader (Berthold). The luminescence measurement was done for 5 sec using 2 sec delay.
779 In addition, 50µl of the lysate were assessed for GFP fluorescence. The luciferase reading was normalized over
780 the GFP results for each well. Data is shown as fold changes over the control plasmid.
781
782 CRISPR-Cas9 editions of hiPSCs
783 CRISPR-Cas9 editing was used to create genomic deletions of the *ZBTB16* exon 2 and of approximately 400 bp of
784 the regulatory element centered on rs648044 an intronic *ZBTB16* variant. Genome editing was done by
785 electroporation of gRNA pairs (crRNA/tracrRNA duplexes, alt-CRISPR IDT) and recombinant S.P. HiFi Cas9 V3
786 nuclease (IDT DNA Technologies, 1081060). crRNAs were designed using the Benchling webtool and analysed for
787 self- or heterodimers using the IDT OligoAnalyzer™ tool (Table S21). To delete the region of interest, 300,000 No.1
788 iPSCs were transfected with 35pmol of each gRNA (crRNA/tracrRNA duplex 1:1 in 1x Arci annealing buffer
789 (STEMCELL Technologies, 76020), IDT DNA Technologies), 40pmol of Cas9 and 100pmol of electroporation
790 enhancer (IDT DNA Technologies, 1075915) in 26.57µl of the P3 primary cell 4D_X Kit S (Lonza, V4XP-3032)
791 using the 4D-Nucleofector X Unit (Lonza, AAF-1003X) with the CA-137 program. Edited cells were plated into one
792 well of 24-well plate coated with Matrigel 1:100 and cultured in supplemented mTESR1 Basal Medium and, for the
793 day of the edition, with RevitaCell (1:100)) at 37°C with 5% $CO_2$. For control editions, cells were electroporated with
794 Cas9 without the addition of gRNAs. The next day the medium was changed to supplemented mTESR1 and cells
795 were propagated approximately for 2-3 days till they reached 80-90% confluence. Next, cells were passaged into a
796 well of a 6-well plate coated with Matrigel using Gentle Cell Dissociation Reagent and propagated until confluence.
797 Subsequently, 89.5% of the cells were expanded, 10% of them were taken for bulk genotyping analysis and 0.5%
798 were plated in a well of a 6-well plate coated with Matrigel to generate single-cell-derived clonal cell lines. Bulk and
799 single cell DNA extraction was done using 30µl of QuickExtract DNA Extraction Solution (Lucigen, QE09050).
800 Briefly, cells were dissociated, pelleted, resuspended in the extraction solution and incubated at 65 °C for 10 min
801 and 98 °C for 5 min. PCR was performed using the primers in Table S19, the Q5 high fidelity master mix (New
802 England Biolabs, M0494S) and 40ng of cell extract in a total volume of 10 µl. The thermal cycling profile of the PCR
803 was: 98 °C 30 s; 35 ×(98° 10 s, 65 °C 15 s, 72 °C 60 s); 72 °C 2 min. Automated electrophoresis technique (DNA
804 screen tape analysis, Agilent) and Sanger sequencing (Eurofins, primers in Table S19) were used to confirm the
805 presence of CRISPR-Cas9-mediated knockout mutants in the bulk population and the single clones. For the
806 *ZBTB16* exon 2 edition we selected a heterozygous KO cell line (termed $ZBTB16^{+/-}$ and $ZBTB16^{+/+}$ for the control
807 edition) showing by western-blot analysis a ~46% reduction in protein expression (Table S18). The rs648044 is a
808 heterozygous SNP in the iPSC cell line used ($rs648044^{G/A}$). From the edited single clones, we selected a
809 heterozygous KO cell line of the enhancer element harboring the A genotype (termed $rs648044^{G/-}$ and $rs648044^{G/A}$
810 for the control edition). The effect of the KO on *ZBTB16* expression was assessed by RT- qPCR in veh and dex
811 conditions and using *POLR2A* and *YWHAZ* for normalization (Table S19).

812
813 Flow Cytometry
814 No.1- ZBTB16$^{+/+}$ and ZBTB16$^{+/-}$ hCOs were collected for Flow Cytometry analysis (FCa) at day 50 after 7 days of
815 treatment with veh or 100nM dex and/or 1µM of the GR antagonist RU-486 (Selleck, S2606). Three to four samples
816 per batch were analysed and each sample contained two individual hCOs. hCOs were enzymatically dissociated
817 with accutase supplemented with DNase I (ThermoFisher Scientific, EN0521) at 37°C for maximum 40 min. During
818 incubation, every 10 min the hCOs were additionally manually dissociated with a P1000 pipette. Once dissociated,
819 the hCOs were centrifuged for 5 min at 300g and the pellet was resuspended in PBS. Next, cells were centrifuged
820 and the cell pellets were fixed with 70% EtOH at -20°C for one hour. Subsequently, After the addition of 5ml washing
821 buffer (PBS + 1% FBS) fixed cells were centrifuged for 30 min, at 4°C and 500g. The cell pellet was resuspended
822 in 200µl staining solution (wash buffer supplemented with anti-PAX6 and anti-EOMES, Table S18) and incubated
823 for 30 min on ice. After the primary antibody incubation, 1ml of washing buffer was added and the stained cells
824 were centrifuged for 30 min, at 4°C, at 500g. The cell pellet was resuspended in 200µl secondary antibody staining
825 solution (wash buffer supplemented with anti-rabbit 488, anti-sheep 594 and DAPI, Table S18) and incubated for
826 30 min on ice. The stained cells were filtered through an 100µm cell strainer and diluted in additional 200µl wash
827 buffer. FCa was performed at a FACS Melody (BD) in BD FACS Flow TM medium, with a nozzle diameter of 100
828 *µ*m. For each run, 20,000 cells were analyzed. For the 488 fluorophore we used the 488nm laser coupled with the
829 530/30 filter and for the 594 fluorophore we used the 561nm laser coupled with the 613/18 filter. *Gating strategy*:
830 SSC-A/FSC-A gates were used to exclude cell debris and FSC-H/ FSC-W to collect single cells. Gating for
831 fluorophores was done using samples stained with secondary antibody only. The flow rate was set below 30
832 events/s. Further analysis was done using the software of the FACS Melody (BD) and the online free software
833 Floreada.io.
834
835 Targeted Bisulfite Sequencing
836 Targeted bisulfite sequencing was performed following the original protocol[40]. DNA was isolated from day 50 hCOs
837 that were treated with 100nM dex or veh for 7 days with the NucleoSpin Genomic DNA kit (Macherey-Nagel).
838 Bisulfite treatments were performed in triplicate for 200ng of DNA from each sample with the EZ DNA Methylation
839 Kit (Zymo Research, D5001) and then pooled to run one PCR amplification per amplicon in order to reduce cost
840 and maximize the number of samples per sequencing run. Twenty nanograms of bisulfite-converted DNA and 49
841 amplification cycles were then used for each PCR amplification (Table S9) with the Takara EpiTaq HS Polymerase
842 (Clontech, R110A). PCR amplicons were then quantified with an automated electrophoresis technique (2200 DNA
843 screen tape analysis, Agilent) and pooled in equimolar quantities for each sample. AMPure XP beads (Beckman
844 Coulter, A63880) were used for a double size selection (200–500 bp) to remove primer dimers and high molecular
845 DNA fragments. Libraries were generated using the TruSeq DNA PCR-Free HT Library Prep Kit (Illumina,
846 20015963) according to the manufacturer's instructions. Each library was quantified with the Qubit® 1.0
847 (ThermoFisher Scientific), normalized to 4 nM and pooled. Library concentration and fragment sizes were checked
848 with the Agilent's 2100 Bioanalyzer (Agilent Technologies) and quantitative PCR using the Kapa HIFI Library
849 quantification kit (Kapa Biosystems, KK4824). Paired-end sequencing was performed on an Illumina MiSeq
850 Instrument (Illumina) with their MiSeq Reagent Kit v3 (MS-102-3001, 2Å~ 300 cycles) with the addition of 15% of
851 PhiX Control v3 library (Illumina, FC-110-3001) generating 300bp long paired-end reads. Reads were processed
852 as described by Roeh *et al.*[40]. In brief, read quality was verified using FastQC[64], and cutadapt v1.11[76] was applied
853 to trim reads. Subsequently, reads were aligned to a restricted reference consisting of the amplicon sites using
854 Bismark v0.18.2[77]. Paired-end reads were stitched together using an in-house perl script. Using the R package
855 methylKit v.1.6.3[78] increasing Phred score quality cutoff to 30, methylation levels were extracted. Further filtering

856 was conducted in R. We excluded artifacts on a per sample basis, including low-coverage amplicons (sequencing
857 coverage < 1000, 0 samples excluded) and samples with bisulfite conversion efficiency lower 95% (0 samples
858 excluded). To test for significance, individual CpGs of the same enhancer element were tested with two-way ANOVA
859 and corrected for multiple comparisons with the two-stage step-up method of Benjamini, Krieger and Yekutieli[79].
860
861 Methylation analysis by Bisulfite Pyrosequencing
862 DNA was isolated from day 50 hCOs that were treated with 100nM dex or veh for 7 days with the NucleoSpin
863 Genomic DNA kit (Macherey-Nagel). Bisulfite treatments were performed in triplicate for 300ng of DNA from each
864 sample with the EZ DNA Methylation Kit (Zymo Research, D5001) and then pooled to run one PCR amplification
865 per amplicon in order to reduce cost and maximize the number of samples per sequencing run. Twenty nanograms
866 of bisulfite-converted DNA and 45 amplification cycles were then used for each PCR amplification (Table S9) with
867 the PyroMark PCR Kit (Qiagen, 978703). Pyrosequencing primers were designed with the MethMarker software
868 and carried out on a PyroMark Q48 Autoprep using PyroMark Q48 Magnetic Beads (cat. no. 974203), PyroMark
869 Q48 Discs (cat. no. 974901) and PyroMark Q48 Absorber Strips (cat.no. 974912), according to the manufacturer's
870 recommendations. To test for significance, individual CpGs were tested with two-way ANOVA and corrected for
871 multiple comparisons with the two-stage step-up method of Benjamini, Krieger and Yekutieli[79].
872
873 HPS0076 chronic single-cell dataset
874 We generated and analyzed a 10x 3' v2 scRNA-seq of 70 days old cerebral organoids (HPS0076 derived) treated
875 with 100nM of dexamethasone for 10 days prior to collection dataset to validate our findings using single-cell
876 transcriptomics. This dataset contained 3794 control cells and 8539 treated cells. We used the MAST R package
877 to compute differential expression between treatment and control for each of the 8 cell-types in the dataset. For
878 this, we only used cells from samples with more than 10 cells in the dataset. We furthermore removed any genes
879 which were expressed in less than 5% of the cells and controlled for the number of expressed genes in the
880 expression model. We used the likelihood ratio test to compute the statistical significance of differential expression
881 and corrected for multiple testing using FDR correction. We adhered to the filtering and testing procedure when we
882 computed differentially expressed genes between ZBTB16 positive and negative cells in the combined population
883 of vehicle- treated Radial Glia and Intermediate Progenitor cells. For the differential testing procedure between
884 treatment and control in cells positive for PAX6 and EOMES, we did not apply the filtering of samples which do not
885 contain more than 10 cells due to low cell numbers in this case.
886 For Gene Set Enrichment Analysis, we used the R package Cluster Profiler (release 3.17)[80,81] and plotted the results
887 using EnrichPlot[82].
888
889 *No1 acute single-cell dataset*
890 Uniform Manifold Approximation and Projection plots (UMAP)[83] were used to visualize the expression of five genes
891 (*ZBTB16, PAX6, TSC22D3, KLF9, HEYL*) in a previously published single-cell RNA seq dataset (Cruceanu et al.,
892 AJP, 2022[18]). Specifically, gene expression was plotted in the day 30 subsets from cell-line 1 of the aforementioned
893 dataset using the SCANPY[84] python package. The software environment and data processing used to produce
894 these Figure s was identical to the environment and processing steps used to produce expression-UMAPs in
895 Cruceanu et al., AJP, 2022[18]. Using the same data subset, the number of cells positive (>0 raw counts) and negative
896 (0 raw counts) for the five genes were computed across the cell-type clusters defined in the associated publication.
897 The percentages of the positive, for each gene, cells in each cluster depicted in Figure 1j were calculated as a
898 fraction of the total cells positive for each gene in all clusters using the Wilson/Brown method with 95% confidence
899 intervals.

900
901 STARR (Self-Transcribing Active Regulatory Region sequencing)-qPCR
902 *rs648044 cloning into STARR reporter plasmid:* For the STARR-qPCR assay, candidate sequences are cloned in
903 the 3'-UTR of the sgGFP reporter gene driven by the SCP1 minimal promoter[85]. Once transfected into GR
904 expressing cells, active regulatory elements would modulate GFP expression under dex treatment[86]. 201bp long
905 DNA inserts (gblock, IDT) containing 200 bp putative regulatory element centered on the rs648044 (reference and
906 alternative allele) and flanked by 15bp sequence homologous to the STARR reporter construct (Table S19) were
907 inserted by in-Fusion HD Cloning Plus into the human STARR-seq vector digested with SalI and AgeI following the
908 manufacturer's instructions (Takara Bio, 102518). The inserts had additionally 2bp to reconstitute the AgeI and SalI
909 restriction sites lost during cloning. Subsequently, the constructs were transformed into Stellar™ competent cells
910 (Takara Bio, 636763) and grown for 16 h on agar plates containing 100µg/ml ampicillin. Single colonies were picked,
911 plasmidic DNA was isolated with Qiagen plasmid kits (12123, 12143) and the genotype was checked with Sanger
912 sequencing (Table S19).
913 *U2OS-GR18 cells transfection:* U2OS cells stably transfected with rat GRα (GR18 cells)[87] were cultured in
914 Dulbecco's Modified Eagle Medium- high glucose supplemented (Gibco™, 11965084) with 10% FBS (Gibco™,
915 16141-061) and 1x Antibiotic-Antimycotic (Gibco™, 15240-062). Two million cells were transfected with 2µg of
916 plasmid in triplicates using the Amaxa Nucleofector II Kit V and program X-001 (Lonza Bioscience). After 16 h cells
917 were treated with 100nM dex or veh for four h. RNA was isolated with the RNeasy Mini extraction kit (Qiagen,
918 74104) according to the manufacturer's instructions.
919 *cDNA conversion and qPCR:* cDNA was generated using two gene specific primers for plasmid GFP and RPL19
920 as endogenous control (Table S19) and the Quantitect Reverse Transcriptase (Qiagen) kit following manufacturer's
921 instructions. Regulatory elements activity was assessed with qPCR using primers for RPL19 and GFP (Table S19).
922 The qPCR was analysed with the relative quantification method and GFP expression was normalized over the
923 RPL19 expression. Data are shown both as expression values ($2^{-DCt}$) and as fold changes of the expression values
924 (dex/veh).
925
926 Mendelian randomization analysis (MRa) and Phenome-wide association (PheWAS) study
927 All processing and analysis were conducted using R software[88]. To assess the potentially causal effect of ZBTB16
928 on a range of phenotypes, rs648044 was used as genetic proxy with log fold-changes of the effect allele (A),
929 averaged over STARR-qPCR experiments, (β= 1.475794, SE= 0.1015) used as exposure effect and variance
930 estimates.
931
932 *Outcome phenotype selection:* Outcome phenotypes were selected from the MRC IEU OpenGWAS platform
933 focusing on phenotype batches originating from the UK Biobank study, the NHGRI-EBI GWAS Catalog, and a
934 GWAS on brain imaging phenotypes based on UK Biobank data (Table S13)[89–92]. From the initial phenotype list
935 originating from these batches, 8979 phenotypes from GWAS of European populations were selected after filtering
936 out duplicates and phenotypes not of interest to this study (e.g., *"*Patient Care Technician r*esponsible for patient*
937 *data" or "Day-of-week questionnaire completion requested").* Duplicates were filtered using a semi-automated
938 procedure including deletion of phenotypes with identical names and smaller GWAS sample size as well as manual
939 filtering of phenotypes with high similarity in trait names (quantified using the restricted Damerau-Levenshtein
940 distance >0.8 implemented in the stringdist package)[93]. This procedure resulted in a final phenotype list of 7,503
941 phenotypes.
942

943 *Mendelian randomisation analysis (MRa):* The *TwoSampleMR* package was used for MRa[94]. Outcome data for
944 rs648044 were extracted from phenotype summary data, which were available for 7,323 outcomes, and effect and
945 reference alleles were harmonised with exposure data. Wald ratio MRa estimation was applied as method of choice
946 for single-SNP MRa for all remaining outcome phenotypes[95]. To account for the multiple comparisons, P-values
947 from all 7,323 comparisons were corrected using the Benjamini-Hochberg method[96]. In results visualizations, we
948 also provide the Bonferroni-corrected multiple comparison threshold as reference[97].
949 *Illustration of PheWAS associations*: Significant phenome-wide associations with brain region phenotypes were
950 illustrated by overlaying human brain atlas regions as proxies of the regions of interest onto the MNI template in
951 MRIcroGl (version v2.1.58-0, https://www.nitrc.org/projects/mricrogl/). Due to the different analysis streams and
952 granularities of the significant brain phenotypes, different atlases were used to portray the results. For illustration
953 purposes, regions taken from probabilistic atlases were thresholded at 10%. As a proxy for the circular anterior
954 insular cortex thickness, we used the anterior insula of the "Hammersmith atlas"[98]. Medial lemniscus, cingulate
955 gyrus part of cingulum, cingulum hippocampus, uncinate fasciculus, posterior limb of internal capsule, inferior
956 fronto-occipital fasciculus, uncinate fasciculus, anterior corona radiata and the corticospinal tract were portrayed
957 using the JHU ICBM DTI 81 white matter labels[99], the acoustic radiation was visualized using the Juelich histological
958 atlas[99], the inferior longitudinal fasciculus, and the thalamic radiation by the JHU White Matter Tractography[100] and
959 the superior thalamic radiation by the XTRACT HCP Probabilistic tract atlas[101].
960 Scripts and data for the MRa-PheWAS analyses are openly available via https://osf.io/4ud6q/ for full transparency.
961
962 Intra-Uterine prospective pregnancy cohort study
963 *Study Cohort:* The Intra-Uterine sampling in early pregnancy (ITU) is a prospective pregnancy cohort study with the
964 overarching aim to unravel maternal-placental-fetal mechanisms involved in the programming of health and
965 disease[52]. It comprises 943 women and their singleton children born alive in Finland between 2012-2017. The
966 women were recruited at the voluntary national 21-trisomy screen, offered to all pregnant women at gestational
967 weeks 9 to 21. Of these women, 543 (57.6%) were referred for fetal chromosomal testing at Helsinki and Uusimaa
968 Hospital District Fetomaternal Medical Center (FMC) and thereafter cleared for fetal chromosomal abnormality. The
969 rest, 400 (42.4%) women, had a negative 21-trisomy screen result and were not referred for fetal chromosomal
970 testing.
971
972 *Ethics Approval:* The ITU study was conducted according to the World Medical Association's Declaration of Helsinki
973 and the research protocol was approved by the ethics committee of the Helsinki and Uusimaa Hospital District
974 (approval date: 06.01.2015, reference number: 269/13/03/00/09). All women provided written informed consent. In
975 compliance with the General Data Protection Regulation of the European Union, the personal data of all participants
976 were de-identified, protected at all times, and confidentiality agreements were signed by all personnel with ITU data
977 access.
978
979 *Data availability:* A complete set of salivary cortisol, fetal rs648044 genotype (genotype frequencies of AA = 0.234,
980 GG = 0.284, AG = 0.482, Hardy-Weinberg-Equilibrium [HWE] p = .630), and child neuropsychological assessment
981 at 35.6 months of age (range 24.5 to 42.5) was available for 246 mother-child dyads (46.7% female sex) before
982 and for 221 mother-child dyads (49.1% female sex) after gestational week 28.
983
984 *Salivary Cortisol Assessment:* Salivary cortisol sample collection, storage, and competitive enzyme immunoassay
985 were previously described[52]. Briefly, mothers collected saliva in early (<22 weeks, T1), mid- (22-35 weeks, T2), and
986 late pregnancy (≥36 weeks, T3) when waking up (S1), 15 (S2) and 30 min (S3) thereafter; at 10 am (S4), noon

(S5), 5 pm (S6), and when going to sleep ("lights out", S7). Gestational week at assessment was computed using the ultrasound-based date of conception and self-reported date of cortisol assessment.

Salivary cortisol samples were available for 690 women (307 with and 383 without chromosomal testing) of which 15 were excluded due to corticosteroid treatment[102] resulting in a total of 9,992 (70.49%) out of the maximum number of 14,175 samples in 675 women. Samples measured in duplicate were averaged and those with a coefficient of variation greater than 0.25 (1.6%, 164/9,992) excluded. Cortisol values below the lower limit of the assay range were truncated at 0.05 $\mu$g/L (2.4%, 240/9,992, no values fell above the upper limit). For some women, multiple assessment days (i.e., 24) fell into the same pregnancy stage and only the one with most complete observations, protocol adherence, or absence of day-specific outliers (i.e., >2SD of the day-specific mean) was kept, leading to the exclusion of 159 samples. For 6 women, date records were missing, and their 89 samples were excluded. Further exclusion criteria were self-reported illness on the day of sampling (89 samples, leading to the exclusion of all samples of 2 women), getting up before the first sample (108 samples), sampling of S2 or S3 more than 60 min after awakening (10 samples), or S4 sampling within the first 60 min after awakening (17 samples). Missing sampling times (0.1%, 19/9,992) were imputed according to sampling protocol for S2 to S6 or sample median for S1 and S7. The distribution of the cortisol samples was positively skewed, and thus natural log+1 transformed. To further reduce skewness, outliers (i.e., >4 SD pregnancy stage-specific mean) were winsorized (9 samples).

The resulting dataset consisted of 9,356 samples from 667 women (292 with and 375 without chromosomal testing). Of these, 589 provided salivary samples before gestational week 28 (range 12.3 to 27.9 weeks) and 499 after gestational week 28 (range 28.14 to 41.3 weeks). Total cortisol output per pregnancy stage was estimated based on the area under the curve with respect to ground (AUCg) of all seven saliva samples using the trapezoid rule[103]. When multiple occasions fell into the same gestational interval (i.e., gestational week <28 or >28 weeks), the total cortisol output and gestational week at assessment were averaged.

*Fetal Genotypes:* DNA was extracted from cord blood leucocytes using a bead-based method optimised by tissue type (Chemagic 360, Perkin Elmer) and genotyping performed on Illumina GSA-24v2-0 A1 arrays according to the manufacturer's guidelines. Genotyping quality control and imputation were previously described in Kvist et al., 2022[52]. In total, the rs648044 genotype was available for 446 (genotype frequencies of AA = 0.226, GG = 0.285, AG = 0.489, HWE p = .704) out of a maximum of 944 samples.

*Child Neuropsychological Assessment*: At 35.48 months (range 24.5 to 42.5 months) follow-up, children's cognitive skills were assessed by trained psychology students (supervised by a clinical pediatric neuropsychologist) using the Bayley-III screening test[53]. The Bayley-III is a norm-referenced test designed to identify infants and toddlers at risk for developmental delay. Scores were calculated using normative data tailored for exact age, with higher scores indicating better performance. The Bayley cognitive assessment was available for n = 618 (50.5% female) out of a maximum of 944 children. Neurodevelopmental delay was defined as 1SD below the sample mean.

*Maternal and child covariates:* All mothers consented to link their data to Finland's detailed nationwide registers. Maternal sociodemographic and pregnancy characteristics used in this study included maternal age at delivery [years], parity [nulli-/multiparous], whether the mother was referred for fetal chromosomal testing [yes vs no], maternal education [primary/applied university/university education], which was self-reported in early pregnancy, and pre-pregnancy Body Mass Index [BMI, weight (kg)/height^2 (m^2)] verified by measurement in the first antenatal clinic visit between 7-10 gestational weeks. Child characteristics included gestational age at delivery and child sex.

1031 *Logistic regressions: Binomial* logistic regressions were run using the "glm" function of the "stats" package in R
1032 (version 3.6.1)[88]. We tested the association of the interaction effect of mean cortisol * rs648044 A allele on delay in
1033 cognitive performance as defined by the Bayley cognitive subscale, using the following covariates: gestational week
1034 at cortisol assessment, child sex, child age when the Bayley questionnaire was done, gestational age at birth,
1035 maternal age and education, parity, maternal body mass index and case vs control as women were either recruited
1036 at routine care (controls) or after referral for chromosomal testing (cases). Cases all tested negative for
1037 chromosomal abnormality). The plot on Figure 6e was done using the "ggplot2" package[104] in R.
1038
1039
1040 **Quantification and Statistical analysis**
1041 Image analysis and Quantifications
1042 Immunostained fluorescent staining was visualized using a Leica laser-scanning microscope and analyzed with FIJI
1043 ((Fiji Is Just) ImageJ 2. 1. 0/1.53c; Java 1. 8. 0_172[64 bit])[105]. For analysis of the hCOs, we included ventricles that
1044 fulfilled the following criteria: clear ventricular structure with elongated, radially-organized cells surrounding the
1045 ventricular zone (VZ- determined with DAPI staining), at least one cell electroporated in the VZ (for electroporation
1046 experiments) and expression of PAX6 and EOMES to define dorsal cortical ventricles. Cell counting was performed
1047 in one representative plane of a z stack using the cell counter tool in FIJI. For electroporations binning analysis was
1048 done.
1049 *Electroporations on hCOs*: For each experiment, at least seven independent ventricles from five different HPS0076-
1050 hCOs generated in three independent preparations grown in different times were analyzed. Analysis of the ZBTB16
1051 phenotype in the electroporation experiments was performed by always comparing hCOs electroporated with
1052 ZBTB16-F2A-GFP plasmid vs F2A-GFP control plasmid in the same batch. Throughout the area of the
1053 electroporation, bins were set as follows: the maximal distance between the most migrated GFP-positive cell and
1054 the apical surface of the ventricle with the first GFP-positive cells was measured and divided into three equally-
1055 heighted bins. Bin A is mainly comprised of the VZ, bin B of the outer-most basal part of the VZ and the SVZ and
1056 bin C of the CP. As normalization we used the number of GFP-positive cells in total or per bin as specified in each
1057 section.
1058 *Dexamethasone effects on hCOs*: For each experiment, at least twelve independent ventricles from six different
1059 HPS0076-hCOs and at least five independent ventricles from three different No.1-hCOs, generated in two
1060 independent preparations for Line-1 and in one preparation from Line-2 iPSCs grown in different times were
1061 analyzed. Analysis of the dex phenotype was performed by always comparing hCOs grown in parallel in the same
1062 batch. For analysis of the dex effects in hCOs, VZ and SVZ (subventricular like-zone) were defined by the cell
1063 shape and proximity to the apical zone. The VZ area presented elongated, radially-organized cells positive for radial
1064 glia markers (PAX6, SOX2) but not for basal progenitors' markers (EOMES). The area on top, assigned as SVZ,
1065 was positive for basal progenitor markers. Areas were defined and measured in FIJI using the ROI Manager tool.
1066 As normalization we used the measured area surface.
1067 *In utero electroporations of fetal mice*: For each experiment and condition, at least eight mouse cortical sections
1068 from five different embryos collected from two littermate mothers were analyzed. For analysis of the *in utero*
1069 electroporations in mice, we used binning analysis. We chose a cortical column that had the majority of
1070 electroporated cells and we set the bins as follows: the maximal distance between the most migrated GFP-positive
1071 cell in the cortical plate and the apical surface of the ventricle was measured and divided by five. The width of the
1072 bin was the width of the 40x lens image and it was the same for all sections and mice. As normalization we used
1073 the number of GFP-positive cells in total or per bin as specified in each section.
1074

1075 Statistics & Plots
1076 The statistical analysis was performed in GraphPad Prism (Version 9. 1.0 (2021)). Datasets were tested for
1077 normality with a D'Agostino & Pearson K2 test[106]. Groups were then compared with a two-tailed Mann-Whitney test
1078 or a one-way or a two-way ANOVA with multiple comparisons corrected with the two-stage step-up method of
1079 Benjamini, Krieger and Yekutieli[79], according to the type of data and their distribution. More specifically, p-values
1080 for Figures: 1f, 3e&f, 4c,e&g, 5c,e&i, 6b and for Supplemental Figures: 1a&b, 3c&e, 7c, 9b, 10a,b,e,g,j&l, 11b,
1081 12a,d&e were calculated using two-way ANOVA with Benjamini, Krieger and Yekutieli multiple testing correction.
1082 P-value for Figure 2f was calculated using one-way ANOVA with Benjamini, Krieger and Yekutieli multiple testing
1083 correction. P-values for Figures: 1c, 2e, 3c, 5h&i and for Supplemental Figures: 3b,d&e, 5b&d, 8b&d, 10d,i&k, 12b
1084 were calculated using Mann–Whitney (two-tailed) comparison between the two treatment/electroporation groups
1085 (veh-dex or ZBTB16 overexpression plasmid- control plasmid). On the plots, the p-values depicted are either the
1086 Welch's t-test p-value, the Mann-Whitney comparison p-value or for the ANOVAS the corrected post-hoc p-values.
1087 For each statistical test the N equals the dots depicted in each plot.
1088 Dots in plots of Figures: 1c&f, 3c,e&f and of Supplemental Figures: 1a&b, 5d, 7c, 8b&d represent individual
1089 ventricles. Specifically, for HPS0076 hCOs results in Figure 1c&f and for Supplemental Figure 1a,b dots represent
1090 individual ventricles from six different HPS0076-hCOs generated in two independent preparations grown in different
1091 times. For No1 hCOs results in Figure 1c,f dots represent individual ventricles from three different No.1-hCOs
1092 generated in one preparation. For Figure 3c,e&f and for Supplemental Figure 7c dots represent individual ventricles
1093 from at least five different HPS0076-hCOs generated in three independent preparations grown at different times.
1094 For Supplemental Figure 5d dots represent individual ventricles from three different hCOs generated in two
1095 independent preparations per iPSC line grown at different times. For Supplemental Figure 8 dots represent
1096 individual ventricles from 4 different hCOs per condition and per genotype generated in one preparation for each
1097 genotype.
1098 Dots in plots of Figures: 2e,f, 4e,g, 6b and of Supplemental Figures: 2c,e, 3b, 5b, 12a,e,f represent replicates each
1099 containing RNA/DNA/protein/cells extracted from a pool of two to three organoids each, i.e, 3 pools each containing
1100 2 to 3 organoids so 6 to 9 organoids in total. More specifically, dots and western lanes in Figures 2e,f and 4b
1101 represent protein and RNA expression values from an isolate of a pool of three hCOs each. The hCOs were
1102 generated in two independent preparations grown in different times per iPSC line. For Figure 4e,g dots represent
1103 FCa results from an isolate of a pool of two hCOs each. The hCOs were generated in two independent preparations
1104 per iPSC line grown at different times. For Figure 6b and for Supplemental Figure 12a results of two or three
1105 replicates for dex respectively and 3 for dmso are depicted and they represent methylation levels from an isolate of
1106 a pool of two hCOs each. For Supplemental Figures 2c,e and 3b dots represent FCa results from an isolate of a
1107 pool of two hCOs each. The hCOs were generated in one preparation for panel 2e and in two preparations for panel
1108 3b and 2c. For Supplemental Figure 5b dots represent RNA expression values from an isolate of a pool of two
1109 hCOs each. The hCOs were generated in two independent preparations grown in different times per iPSC line. For
1110 Supplemental Figure 12e,f dots represent RNA expression values or fold changes from an isolate of a pool of two
1111 hCOs each. The hCOs were generated in one preparation per iPSC line.
1112 Dots in plots of Figure 5 and Figure S10 and S11 represent individual embryos. Each dot represents average counts
1113 from at least two cortical sections from one embryo. Embryos collected from two independent mothers were
1114 analysed for each staining.
1115 For Figure S11 dots represent luciferase activity values of cells from independent cell culture wells for each
1116 condition and promoter.
1117 Dots in Figure S12a,b represent RNA expression values or fold changes from isolates of independent cell culture
1118 wells for each genotype and treatment.

1119 Box and whisker plots represent 25th to 75th percentile of the data with the center line representing the median and
1120 whiskers representing minima and maxima. Bar plots with error bars showing standard error of the mean (SEM).
1121 Plots and statistics for all Figures were generated using the GraphPad Prism 9 software.
1122 Significance: ****: p <=0.0001, ***: p <=0.001, **: p <=0.01, *: p <=0.05, ns: p >0.05.
1123

1124 **References**


1125 1. Barker, D.J.P. (2004). The developmental origins of chronic adult disease. Acta Paediatr Suppl, 26–33.
1126 10.1080/08035320410022730.
1127 2. Monk, C., Lugo-Candelas, C., and Trumpff, C. (2019). Prenatal Developmental Origins of Future
1128 Psychopathology: Mechanisms and Pathways. Annu Rev Clin Psychol *15*. 10.1146/annurev-clinpsy-
1129 050718-095539.
1130 3. Krontira, A.C., Cruceanu, C., and Binder, E.B. (2020). Glucocorticoids as Mediators of Adverse Outcomes
1131 of Prenatal Stress. Trends Neurosci *43*, 394–405. 10.1016/j.tins.2020.03.008.
1132 4. Carson, R., Monaghan-Nichols, A.P., DeFranco, D.B., and Rudine, A.C. (2016). Effects of antenatal
1133 glucocorticoids on the developing brain. Steroids *114*, 25–32. 10.1016/j.steroids.2016.05.012.
1134 5. Edwards, P.D., and Boonstra, R. (2018). Glucocorticoids and CBG during pregnancy in mammals: diversity,
1135 pattern, and function. Gen Comp Endocrinol *259*, 122–130. 10.1016/j.ygcen.2017.11.012.
1136 6. Harris, A., and Seckl, J. (2011). Glucocorticoids, prenatal stress and the programming of disease. Horm
1137 Behav *59*, 279–289. 10.1016/j.yhbeh.2010.06.007.
1138 7. Lajic, S., Karlsson, L., and Nordenström, A. (2018). Prenatal Treatment of Congenital Adrenal Hyperplasia :
1139 Long-Term Effects of Excess Glucocorticoid Exposure. Hormone Research in Pediatrics.
1140 10.1159/000485100.
1141 8. Committee on Obstetric Practice (2017). Antenatal Corticosteroid Therapy for Fetal Maturation. Obstetrics
1142 and Gynecology *130*, 102–109.
1143 9. Cao, G., Liu, J., and Liu, M. (2022). Global, Regional, and National Incidence and Mortality of Neonatal
1144 Preterm Birth, 1990-2019. JAMA Pediatr, 1–10. 10.1001/jamapediatrics.2022.1622.
1145 10. Chawanpaiboon, S., Vogel, J.P., Moller, A.B., Lumbiganon, P., Petzold, M., Hogan, D., Landoulsi, S.,
1146 Jampathong, N., Kongwattanakul, K., Laopaiboon, M., et al. (2019). Global, regional, and national estimates
1147 of levels of preterm birth in 2014: a systematic review and modelling analysis. Lancet Glob Health *7*, e37–
1148 e46. 10.1016/S2214-109X(18)30451-0.
1149 11. Vidavalur, R., Hussain, Z., and Naveed, H. (2022). Association of Survival at 22 Weeks' Gestation With
1150 Use of Antenatal Corticosteroids and Mode of Delivery in the United States. JAMA Pediatr, 10–12.
1151 12. The RECOVERY Collaborative Group (2020). Dexamethasone in Hospitalized Patients with Covid-19 —
1152 Preliminary Report. N Engl J Med, 1–11. 10.1056/NEJMoa2021436.
1153 13. Mcintosh, J.J. (2020). Corticosteroid Guidance for Pregnancy during COVID-19 Pandemic. Americal
1154 Journal of Perinatology, 809–812.
1155 14. Ninan, K., Liyanage, S.K., Murphy, K.E., Asztalos, E. V, and McDonald, S.D. (2022). Evaluation of Long-
1156 term Outcomes Associated With Preterm Exposure to Antenatal Corticosteroids: A Systematic Review and
1157 Meta-analysis. JAMA Pediatr, e220483. 10.1001/jamapediatrics.2022.0483.
1158 15. Mcewen, B.S., Bowles, N.P., Gray, J.D., Hill, M.N., Hunter, R.G., Karatsoreos, I.N., and Nasca, C. (2015).
1159 Mechanisms of stress in the brain. Nat Neurosci *18*. 10.1038/nn.4086.
1160 16. Malik, S., Vinukonda, G., Vose, L.R., Diamond, D., Bhimavarapu, B.B.R., Hu, F., Zia, M.T., Hevner, R.,
1161 Zecevic, N., and Ballabh, P. (2013). Neurogenesis continues in the third trimester of pregnancy and is

1162 suppressed by premature birth. Journal of Neuroscience *33*, 411–423. 10.1523/JNEUROSCI.4445-
1163 12.2013.
1164 17. Lancaster, M.A., and Knoblich, J.A. (2014). Generation of cerebral organoids from human pluripotent stem
1165 cells. Nat Protoc *9*, 2329–2340. 10.1038/nprot.2014.158.
1166 18. Cruceanu, C., Dony, L., Krontira, A.C., Fischer, D.S., Roeh, S., Di Giaimo, R., Kyrousi, C., Kaspar, L.,
1167 Arloth, J., Czamara, D., et al. (2022). Cell-Type-Specific Impact of Glucocorticoid Receptor Activation on
1168 the Developing Brain: A Cerebral Organoid Study. American Journal of Psychiatry *179*, 375–387.
1169 10.1176/appi.ajp.2021.21010095.
1170 19. Dehay, C., Kennedy, H., and Kosik, K.S. (2015). The Outer Subventricular Zone and Primate-Specific
1171 Cortical Complexification. Neuron *85*, 683–694. 10.1016/j.neuron.2014.12.060.
1172 20. Betizeau, M., Cortay, V., Patti, D., Pfister, S., Gautier, E., Bellemin-Ménard, A., Afanassieff, M., Huissoud,
1173 C., Douglas, R.J., Kennedy, H., et al. (2013). Precursor Diversity and Complexity of Lineage Relationships
1174 in the Outer Subventricular Zone of the Primate. Neuron *80*, 442–457. 10.1016/j.neuron.2013.09.032.
1175 21. Romero, C.D.J., Bruder, C., Tomasello, U., Sanz-anquela, J.M., and Borrell, V. (2015). Discrete domains
1176 of gene expression in germinal layers distinguish the development of gyrencephaly. EMBO J *34*, 1859–
1177 1874.
1178 22. Florio, M., and Huttner, W.B. (2014). Neural progenitors, neurogenesis and the evolution of the neocortex.
1179 Development (Cambridge) *141*, 2182–2194. 10.1242/dev.090571.
1180 23. Matsumoto, N., Tanaka, S., Horiike, T., and Shinmyo, Y. (2020). A discrete subtype of neural progenitor
1181 crucial for cortical folding in the gyrencephalic mammalian brain. Elife, 1–26.
1182 24. Borrell, V., and Götz, M. (2014). Role of radial glial cells in cerebral cortex folding. Curr Opin Neurobiol *27*,
1183 39–46. 10.1016/j.conb.2014.02.007.
1184 25. Silbereis, J.C., Pochareddy, S., Zhu, Y., Li, M., and Sestan, N. (2016). The Cellular and Molecular
1185 Landscapes of the Developing Human Central Nervous System. Neuron *89*, 248.
1186 10.1016/j.neuron.2015.12.008.
1187 26. Cruceanu, C., Ph, D., Dony, L., Sc, M., Krontira, A.C., Sc, M., Fischer, D.S., Sc, M., Roeh, S., and Sc, B.
1188 (2021). Cell-Type-Specific Impact of Glucocorticoid Receptor Activation on the Developing Brain : A
1189 Cerebral Organoid Study. American Journal of Psychiatry, 1–13. 10.1176/appi.ajp.2021.21010095.
1190 27. Liu, T.M., Lee, E.H., Lim, B., and Shyh-Chang, N. (2015). Balancing Stem Cell Self-renewal and
1191 Differentiation with PLZF. Stem Cells, 277–287. 10.1002/stem.2270.
1192 28. Avantaggiato, V., Pandolfi, P.P., Ruthardt, M., Hawe, N., Acampora, D., Pelicci, P.G., and Simeone, A.
1193 (1995). Developmental analysis of murine Promyelocyte Leukemia Zinc Finger (PLZF) gene expression:
1194 implications for the neuromeric model of the forebrain organization. The Journal of Neuroscience *15*, 4927–
1195 4942.
1196 29. Pebworth, M.P., Ross, J., Andrews, M., Bhaduri, A., and Kriegstein, A.R. (2021). Human intermediate
1197 progenitor diversity during cortical development. Proc Natl Acad Sci U S A *118*, 1–10.
1198 10.1073/pnas.2019415118.
1199 30. Hai, L., Szwarc, M.M., Lanza, D.G., Heaney, J.D., and Lydon, J.P. (2019). Using CRISPR / Cas9
1200 engineering to generate a mouse with a conditional knockout allele for the promyelocytic leukemia zinc
1201 finger transcription factor. 1–8. 10.1002/dvg.23281.
1202 31. Stepien, B.K., Vaid, S., and Huttner, W.B. (2021). Length of the Neurogenic Period—A Key Determinant
1203 for the Generation of Upper-Layer Neurons During Neocortex Development and Evolution. Front Cell Dev
1204 Biol *9*, 1–20. 10.3389/fcell.2021.676911.

1205 32. Magrinelli, E., Baumann, N., Wagener, R.J., Glangetas, C., Bellone, C., Jabaudon, D., and Klingler, E.
1206 (2022). Heterogeneous fates of simultaneously-born neurons in the cortical ventricular zone. Sci Rep *12*,
1207 1–11. 10.1038/s41598-022-09740-6.
1208 33. Manuel, M., Georgala, P.A., Carr, C.B., Chanas, S., Kleinjan, D.A., Martynoga, B., Mason, J.O., Molinek,
1209 M., Pinson, J., Pratt, T., et al. (2007). Controlled overexpression of Pax6 in vivo negatively auto- regulates
1210 the Pax6 locus , causing cell-autonomous defects of late cortical progenitor proliferation with little effect on
1211 cortical arealization. Development *555*, 545–555. 10.1242/dev.02764.
1212 34. Sansom, S.N., Griffiths, D.S., Faedo, A., Kleinjan, D., Ruan, Y., Heyningen, V. Van, Rubenstein, J.L., and
1213 Livesey, F.J. (2009). The Level of the Transcription Factor Pax6 Is Essential for Controlling the Balance
1214 between Neural Stem Cell Self- Renewal and Neurogenesis. PLoS Genet *5*, 20–23.
1215 10.1371/journal.pgen.1000511.
1216 35. Elsen, G.E., Bedogni, F., Hodge, R.D., and Bammler, T.K. (2018). The Epigenetic Factor Landscape of
1217 Developing Neocortex Is Regulated by Transcription Factors. Front Neurosci *12*.
1218 10.3389/fnins.2018.00571.
1219 36. Anderson, T.R., Hedlund, E., and Carpenter, E.M. (2002). Differential Pax6 promoter activity and transcript
1220 expression during forebrain development. Mech Dev *114*, 171–175.
1221 37. Tyas, D.A., Simpson, T.I., Carr, C.B., Kleinjan, D.A., Van Heyningen, V., Mason, J.O., and Price, D.J.
1222 (2006). Functional conservation of Pax6 regulatory elements in humans and mice demonstrated with a
1223 novel transgenic reporter mouse. BMC Dev Biol *6*, 1–11. 10.1186/1471-213X-6-21.
1224 38. Provençal, N., Arloth, J., Cattaneo, A., Anacker, C., Cattane, N., Wiechmann, T., Röh, S., Ködel, M.,
1225 Klengel, T., Czamara, D., et al. (2019). Glucocorticoid exposure during hippocampal neurogenesis primes
1226 future stress response by inducing changes in DNA methylation. Proceedings of the National Academy of
1227 Sciences *117*, 201820842. 10.1073/pnas.1820842116.
1228 39. Wiechmann, T., Röh, S., Sauer, S., Czamara, D., Arloth, J., Ködel, M., Beintner, M., Knop, L., Menke, A.,
1229 Binder, E.B., et al. (2019). Identification of dynamic glucocorticoid- induced methylation changes at the
1230 FKBP5 locus. Clin Epigenetics, 1–14.
1231 40. Roeh, S., Wiechmann, T., Sauer, S., Ködel, M., Binder, E.B., and Provençal, N. (2018). HAM-TBS: High-
1232 accuracy methylation measurements via targeted bisulfite sequencing. Epigenetics Chromatin *11*, 1–10.
1233 10.1186/s13072-018-0209-x.
1234 41. Bothe, M., Buschow, R., and Meijsing, S.H. (2021). Glucocorticoid signaling induces transcriptional memory
1235 and universally reversible chromatin changes. Life Sci Alliance *4*, 1–17. 10.26508/lsa.202101080.
1236 42. Klengel, T., and Binder, E.B. (2015). Epigenetics of Stress-Related Psychiatric Disorders and Gene ×
1237 Environment Interactions. Neuron *86*, 1343–1357. 10.1016/j.neuron.2015.05.036.
1238 43. Lee, J.J., Wedow, R., Okbay, A., Kong, E., Maghzian, O., Zacher, M., Nguyen-Viet, T.A., Bowers, P.,
1239 Sidorenko, J., Linnér, R.K., et al. (2018). Gene discovery and polygenic prediction from a genome-wide
1240 association study of educational attainment in 1.1 million individuals. Nat Genet *50*. 10.1038/s41588-018-
1241 0147-3.
1242 44. Okbay, A., Wu, Y., Wang, N., Jayashankar, H., Bennett, M., Nehzati, S.M., Sidorenko, J., Kweon, H.,
1243 Goldman, G., Gjorgjieva, T., et al. (2022). Polygenic prediction of educational attainment within and
1244 between families from genome-wide association analyses in 3 million individuals. Nat Genet *54*.
1245 10.1038/s41588-022-01016-z.
1246 45. Makowski, C., Loughnan, R., Jernigan, T.L., Seibert, T.M., Hagler, D.J., Smeland, O.B., Motazedi, E., Chu,
1247 Y., Lin, A., Hindley, G., et al. (2022). Vertex-wise multivariate genome-wide association study identifies 780

1248 unique genetic loci associated with cortical morphology. Neuroimage, 1–19.
1249 10.1016/j.neuroimage.2021.118603.Vertex-wise.
1250 46. Schiller, B.J., Chodankar, R., Watson, L.C., Stallcup, M.R., and Yamamoto, K.R. (2014). Glucocorticoid
1251 receptor binds half sites as a monomer and regulates specific target genes. Genome Biol *15*, 1–16.
1252 10.1186/s13059-014-0418-y.
1253 47. Smith, D.J., Nicholl, B.I., Cullen, B., Martin, D., Ul-haq, Z., Evans, J., Gill, J.M.R., Roberts, B., Gallacher,
1254 J., Mackay, D., et al. (2013). Prevalence and Characteristics of Probable Major Depression and Bipolar
1255 Disorder within UK Biobank : Cross-Sectional Study of 172 , 751 Participants. *8*, 1–7.
1256 10.1371/journal.pone.0075362.
1257 48. Bartrés-Faz, D., González-Escamilla, G., Vaqué-Alcázar, L., Abellaneda-Pérez, K., Valls-Pedret, C., Ros,
1258 E., and Grothe, M.J. (2019). Characterizing the molecular architecture of cortical regions associated with
1259 high educational attainment in older individuals. Journal of Neuroscience *39*, 4566–4575.
1260 10.1523/JNEUROSCI.2370-18.2019.
1261 49. Ge, T., Chen, C.Y., Doyle, A.E., Vettermann, R., Tuominen, L.J., Holt, D.J., Sabuncu, M.R., and Smoller,
1262 J.W. (2019). The Shared Genetic Basis of Educational Attainment and Cerebral Cortical Morphology.
1263 Cerebral Cortex *29*, 3471–3481. 10.1093/cercor/bhy216.
1264 50. Kim, J.P., Seo, S.W., Shin, H.Y., Ye, B.S., Yang, J.J., Kim, C., Kang, M., Jeon, S., Kim, H.J., Cho, H., et al.
1265 (2015). Effects of education on aging-related cortical thinning among cognitively normal individuals.
1266 Neurology *85*, 806–812. 10.1212/WNL.0000000000001884.
1267 51. Vaqué-alcázar, L., Sala-llonch, R., and Valls-pedret, C. (2017). Differential age-related gray and white
1268 matter impact mediates educational influence on elders ' cognition. Brain Imaging Behav *11*, 318–332.
1269 10.1007/s11682-016-9584-8.
1270 52. Kvist, T., Sammallahti, S., Lahti-Pulkkinen, M., Cruceanu, C., Czamara, D., Dieckmann, L., Tontsch, A.,
1271 Röh, S., Rex-Haffner, M., Wolford, E., et al. (2022). Cohort profile: InTraUterine sampling in early pregnancy
1272 (ITU), a prospective pregnancy cohort study in Finland: Study design and baseline characteristics. BMJ
1273 Open *12*, 1–11. 10.1136/bmjopen-2021-049231.
1274 53. N, B. (2006). Bayley scales of infant and toddler development (Pearson: PsychCorp)
1275 https://doi.org/10.1037/t14978-000.
1276 54. Garcia, M.T., Chang, Y., Arai, Y., and Huttner, W.B. (2016). S-Phase Duration Is the Main Target of Cell
1277 Cycle Regulation in Neural Progenitors of Developing Ferret Neocortex. J Comp Neurol *470*, 456–470.
1278 10.1002/cne.23801.
1279 55. McEwen, B.S., Nasca, C., and Gray, J.D. (2016). Stress Effects on Neuronal Structure: Hippocampus,
1280 Amygdala, and Prefrontal Cortex. Neuropsychopharmacology *41*, 3–23. 10.1038/npp.2015.171.
1281 56. Popoli, M., Yan, Z., McEwen, B.S., and Sanacora, G. (2012). The stressed synapse: The impact of stress
1282 and glucocorticoids on glutamate transmission. Nat Rev Neurosci *13*, 22–37. 10.1038/nrn3138.
1283 57. Melamed, N., Asztalos, E., Murphy, K., Zaltz, A., Redelmeier, D., Shah, B.R., and Barrett, J. (2019).
1284 Neurodevelopmental disorders among term infants exposed to antenatal corticosteroids during pregnancy :
1285 a population-based study. 3–10. 10.1136/bmjopen-2019-031197.
1286 58. Räikkönen, K., Gissler, M., and Kajantie, E. (2020). Associations Between Maternal Antenatal
1287 Corticosteroid Treatment and Mental and Behavioral Disorders in Children Supplemental content. JAMA
1288 *323*, 1924–1933. 10.1001/jama.2020.3937.
1289 59. Tsiarli, M.A., Rudine, A., Kendall, N., Pratt, M.O., Krall, R., Thiels, E., Defranco, D.B., and Monaghan, A.P.
1290 (2017). Antenatal dexamethasone exposure differentially affects distinct cortical neural progenitor cells and

1291 triggers long-term changes in murine cerebral architecture and behavior. Transl Psychiatry.
1292 10.1038/tp.2017.65.
1293 60. Mcewen, B.S. (2005). Glucocorticoids , depression , and mood disorders : structural remodeling in the brain.
1294 Metabolism *54*, 20–23. 10.1016/j.metabol.2005.01.008.
1295 61. Koyanagi-Aoi, M., Ohnuki, M., Takahashi, K., Okita, K., Noma, H., Sawamura, Y., Teramoto, I., Narita, M.,
1296 Sato, Y., Ichisaka, T., et al. (2013). Differentiation-defective phenotypes revealed by large-scale analyses
1297 of human pluripotent stem cells. Proc Natl Acad Sci U S A *110*, 20569–20574. 10.1073/pnas.1319061110.
1298 62. Okita, K., Matsumura, Y., Sato, Y., Okada, A., Morizane, A., Okamoto, S., Hong, H., Nakagawa, M.,
1299 Tanabe, K., Tezuka, K.I., et al. (2011). A more efficient method to generate integration-free human iPS
1300 cells. Nat Methods *8*, 409–412. 10.1038/nmeth.1591.
1301 63. Cárdenas, A., Villalba, A., de Juan Romero, C., Picó, E., Kyrousi, C., Tzika, A.C., Tessier-Lavigne, M., Ma,
1302 L., Drukker, M., Cappello, S., et al. (2018). Evolution of Cortical Neurogenesis in Amniotes Controlled by
1303 Robo Signaling Levels. Cell *174*, 590-606.e21. 10.1016/j.cell.2018.06.007.
1304 64. Andrews Simon, Krueger Felix, Segonds-Pichon Anne, Biggins Laura, Krueger Christel, M.J. (2019).
1305 fastQC. https://www.bioinformatics.babraham.ac.uk/projects/fastqc/.
1306 65. Martin, M. (2011). Cutadapt removes adapter sequences from high-throughput sequencing reads. EMBnet
1307 J *17*, 10–12.
1308 66. Patro, R., Duggal, G., Love, M.I., Irizarry, R.A., and Kingsford, C. (2017). Salmon provides fast and bias-
1309 aware quantification of transcript expression. Nat Methods *14*, 417–419. 10.1038/nmeth.4197.
1310 67. Love, M.I., Huber, W., and Anders, S. (2014). Moderated estimation of fold change and dispersion for RNA-
1311 seq data with DESeq2. Genome Biol *15*, 1–21. 10.1186/s13059-014-0550-8.
1312 68. Saito, T. (2006). In vivo electroporation in the embryonic mouse central nervous system. Nat Protoc *1*,
1313 1552–1558. 10.1038/nprot.2006.276.
1314 69. Buchsbaum, I.Y., Kielkowski, P., Giorgio, G., Neill, A.C.O., Giaimo, R. Di, Kyrousi, C., Khattak, S., Sieber,
1315 S.A., Robertson, S.P., and Cappello, S. (2020). ECE2 regulates neurogenesis and neuronal migration
1316 during human cortical development. EMBO Rep *49*, 1–24. 10.15252/embr.201948204.
1317 70. Klaus, J., Kanton, S., Kyrousi, C., Ayo-Martin, A.C., Di Giaimo, R., Riesenberg, S., O'Neill, A.C., Camp,
1318 J.G., Tocco, C., Santel, M., et al. (2019). Altered neuronal migratory trajectories in human cerebral
1319 organoids derived from individuals with neuronal heterotopia. Nat Med *25*, 561–568. 10.1038/s41591-019-
1320 0371-0.
1321 71. Jobe, A.H., Kemp, M., Schmidt, A., Takahashi, T., Newnham, J., and Milad, M. (2021). Antenatal
1322 corticosteroids : a reappraisal of the drug formulation and dose. Pediatr Res. 10.1038/s41390-020-01249-
1323 w.
1324 72. Kelava, I., Chiaradia, I., Pellegrini, L., Kalinka, A.T., and Lancaster, M.A. (2021). Androgens increase
1325 excitatory neurogenic potential in human brain organoids. 10.1038/s41586-021-04330-4.
1326 73. McManus, J.M., and Sharifi, N. (2020). Structure-dependent retention of steroid hormones by common
1327 laboratory materials. Journal of Steroid Biochemistry and Molecular Biology *198*, 1–19.
1328 10.1016/j.jsbmb.2019.105572.
1329 74. Spoelhof, B., Ray, S.D., and Wayne, F. (2014). Fludrocortisone Cortisol/Hydrocortisone. In Encyclopedia
1330 of Toxicology, pp. 1038–1042. 10.1016/B978-0-12-386454-3.00293-1.
1331 75. Kashiwagi, Y., Kato, N., Sassa, T., Nishitsuka, K., Yamamoto, T., Takamura, H., and Yamashita, H. (2010).
1332 Cotylenin a inhibits cell proliferation and induces apoptosis and PAX6 mRNA transcripts in retinoblastoma
1333 cell lines. Mol Vis *16*, 970–982.
1334 76. Martin, M. Cutadapt removes adapter sequences from high-throughput sequencing reads.

1335 77. Krueger, F., and Andrews, S.R. (2011). Bismark: A flexible aligner and methylation caller for Bisulfite-Seq
1336 applications. Bioinformatics *27*, 1571–1572. 10.1093/bioinformatics/btr167.
1337 78. Akalin, A., Kormaksson, M., Li, S., Garrett-Bakelman, F.E., Figueroa, M.E., Melnick, A., and Mason, C.E.
1338 (2012). MethylKit: a comprehensive R package for the analysis of genome-wide DNA methylation profiles.
1339 Genome Biol *13*. 10.1186/gb-2012-13-10-R87.
1340 79. Benjamini, Y., Krieger, A.M., and Yekutieli, D. (2006). Adaptive linear step-up procedures that control the
1341 false discovery rate. Biometrika *93*, 491–507. 10.1093/biomet/93.3.491.
1342 80. Wu, T., Hu, E., Xu, S., Chen, M., Guo, P., Dai, Z., Feng, T., Zhou, L., Tang, W., Zhan, L., et al. (2021).
1343 clusterProfiler 4.0: A universal enrichment tool for interpreting omics data. The Innovation *2*.
1344 10.1016/j.xinn.2021.100141.
1345 81. Yu, G., Wang, L.-G., Han, Y., and He, Q.-Y. (2012). clusterProfiler: an R Package for Comparing Biological
1346 Themes Among Gene Clusters. OMICS *16*, 284–287. 10.1089/omi.2011.0118.
1347 82. G, Y. (2023). Enrichplot: Visualization of Functional Enrichment Result. R package version 1.20.0.
1348 83. Becht, E., McInnes, L., Healy, J., Dutertre, C.A., Kwok, I.W.H., Ng, L.G., Ginhoux, F., and Newell, E.W.
1349 (2019). Dimensionality reduction for visualizing single-cell data using UMAP. Nat Biotechnol *37*, 38–47.
1350 10.1038/nbt.4314.
1351 84. Wolf, F.A., Angerer, P., and Theis, F.J. (2018). Open Access SCANPY : large-scale single-cell gene
1352 expression data analysis. Genome Biol, 1–5.
1353 85. Arnold, C.D., Gerlach, D., Stelzer, C., Boryń, Ł.M., Rath, M., and Stark, A. (2013). Genome-wide
1354 quantitative enhancer activity maps identified by STARR-seq. Science (1979) *339*, 1074–1077.
1355 10.1126/science.1232542.
1356 86. Schöne, S., Bothe, M., Einfeldt, E., Borschiwer, M., Benner, P., Vingron, M., Thomas-Chollier, M., and
1357 Meijsing, S.H. (2018). Synthetic STARR-seq reveals how DNA shape and sequence modulate
1358 transcriptional output and noise. PLoS Genet *14*, 1–24. 10.1371/journal.pgen.1007793.
1359 87. Rogatsky, I., Trowbridge, J.M., and Garabedian, M.J. (1997). Glucocorticoid receptor-mediated cell cycle
1360 arrest is achieved through distinct cell-specific transcriptional regulatory mechanisms. Mol Cell Biol *17*,
1361 3181–3193. 10.1128/mcb.17.6.3181.
1362 88. Team, R.C. (2017). R: A language and environment for statistical computing. https://www.r-project.org/.
1363 89. Elsworth, B., Lyon, M., Alexander, T., Liu, Y., Matthews, P., Hallett, J., Bates, P., Palmer, T., Haberland,
1364 V., Davey, G., et al. (2020). The MRC IEU OpenGWAS data infrastructure. bioRxiv, 2020.08.10.244293.
1365 90. Bycroft, C., Freeman, C., Petkova, D., Band, G., Elliott, L.T., Sharp, K., Motyer, A., Vukcevic, D., Delaneau,
1366 O., O'Connell, J., et al. (2018). The UK Biobank resource with deep phenotyping and genomic data. Nature
1367 *562*, 203–209. 10.1038/s41586-018-0579-z.
1368 91. Buniello, A., Macarthur, J.A.L., Cerezo, M., Harris, L.W., Hayhurst, J., Malangone, C., McMahon, A.,
1369 Morales, J., Mountjoy, E., Sollis, E., et al. (2019). The NHGRI-EBI GWAS Catalog of published genome-
1370 wide association studies, targeted arrays and summary statistics 2019. Nucleic Acids Res *47*, D1005–
1371 D1012. 10.1093/nar/gky1120.
1372 92. Elliott, L.T., Sharp, K., Alfaro-Almagro, F., Shi, S., Miller, K.L., Douaud, G., Marchini, J., and Smith, S.M.
1373 (2018). Genome-wide association studies of brain imaging phenotypes in UK Biobank. Nature *562*, 210–
1374 216. 10.1038/s41586-018-0571-7.
1375 93. van der Loo, M.P.J. (2014). The stringdist package for approximate string matching. R Journal *6*, 111–122.
1376 10.32614/rj-2014-011.

94. Hemani, G., Zheng, J., Elsworth, B., Wade, K.H., Haberland, V., Baird, D., Laurin, C., Burgess, S., Bowden, J., Langdon, R., et al. (2018). The MR-base platform supports systematic causal inference across the human phenome. Elife *7*, 1–29. 10.7554/eLife.34408.

95. Palmer, T.M., Sterne, J.A.C., Harbord, R.M., Lawlor, D.A., Sheehan, N.A., Meng, S., Granell, R., Smith, G.D., and Didelez, V. (2011). Instrumental variable estimation of causal risk ratios and causal odds ratios in mendelian randomization analyses. Am J Epidemiol *173*, 1392–1403. 10.1093/aje/kwr026.

96. Benjamini, Y., and Hochberg, Y. (1995). Controlling the False Discovery Rate: A Practical and Powerful Approach to Multiple Testing. Journal of the Royal Statistical Society: Series B (Methodological) *57*, 289–300. 10.1111/j.2517-6161.1995.tb02031.x.

97. Bland, j. M., and Altman, D.G. (1995). Multiple significance tests: The Bonferroni method. Bmj *310*, 170. 10.1136/bmj.310.6973.170.

98. Faillenot, I., Heckemann, R.A., Frot, M., and Hammers, A. (2017). Macroanatomy and 3D probabilistic atlas of the human insula. Neuroimage *150*, 88–98. 10.1016/j.neuroimage.2017.01.073.

99. Mori, S., Oishi, K., Jiang, H., Jiang, L., Li, X., Akhter, K., Hua, K., Faria, A. V., Mahmood, A., Woods, R., et al. (2008). Stereotaxic white matter atlas based on diffusion tensor imaging in an ICBM template. Neuroimage *40*, 570–582. 10.1016/j.neuroimage.2007.12.035.

100. Hua, K., Zhang, J., Wakana, S., Jiang, H., Li, X., Reich, D.S., Calabresi, P.A., Pekar, J.J., van Zijl, P.C.M., and Mori, S. (2008). Tract Probability Maps in Stereotaxic Spaces: Analyses of White Matter Anatomy and Tract-Specific Quantification. Neuroimage *32*, 736–740. 10.1016/j.neuroimage.2007.07.053.Tract.

101. Warrington, S., Bryant, K.L., Khrapitchev, A.A., Sallet, J., Charquero-Ballester, M., Douaud, G., Jbabdi, S., Mars, R.B., and Sotiropoulos, S.N. (2020). XTRACT - Standardised protocols for automated tractography in the human and macaque brain. Neuroimage *217*, 1–15. 10.1016/j.neuroimage.2020.116923.

102. Masharani, U., Shiboski, S., Eisner, M.D., Katz, P.P., Janson, S.L., Granger, D.A., and Blanc, P.D. (2005). Impact of exogenous glucocorticoid use on salivary cortisol measurements among adults with asthma and rhinitis. Psychoneuroendocrinology *30*, 744–752. 10.1016/j.psyneuen.2005.03.003.

103. Pruessner, J.C., Kirschbaum, C., Meinlschmid, G., and Hellhammer, D.H. (2003). Two formulas for computation of the area under the curve represent measures of total hormone concentration versus time-dependent change. Psychoneuroendocrinology *28*, 916–931. 10.1016/S0306-4530(02)00108-7.

104. Wickham, H. (2016). ggplot2: Elegant Graphics for Data Analysis. Springer-Verlag New York.

105. Schindelin, J., Arganda-Carreras, I., Frise, E., Kaynig, V., Longair, M., Pietzsch, T., Preibisch, S., Rueden, C., Saalfeld, S., Schmid, B., et al. (2012). Fiji: an open-source platform for biological-image analysis. Nature Methods 2012 9:7 *9*, 676–682. 10.1038/nmeth.2019.

106. Trujillo-Ortiz, A., and Hernandez-Walls, R. (2003). D'Agostino-Pearson's K2 test for assessing normality of data using skewness and kurtosis. 10.13140/RG.2.2.19734.98889.